Onsager loop transition and first-order flux-line lattice melting in high-T_c superconductors

A. K. Nguyen and A. Sudbø

Department of Physics, Norwegian University of Science and Technology, N-7034 Trondheim, Norway

(Received 24 April 1997; revised manuscript received 31 July 1997)

Monte Carlo simulations in conjunction with finite-size scaling analysis are used to investigate the (H,T)-phase diagram in uniaxial anisotropic high-T_c superconductors, both in zero magnetic field ($B=0$) and in intermediate magnetic fields ($0 \ll B \ll B_{c2}$) for various mass anisotropies. The model we consider is the uniformly frustrated anisotropic Villain model, which is dual to the lattice London model with an infinite London penetration length. The quantities we consider are various helicity moduli, the structure function, the specific heat, and the distribution of closed non-field-induced vortex loops as a function of the loop size. In zero magnetic field, and for all anisotropies considered, we find one single second-order phase transition, mediated by an Onsager vortex-loop unbinding transition, or blowout. This is the superconductor–normal-metal transition. A comparison with numerical simulations and a critical scaling analysis of the zero-field loop transition yields the same exponent of the loop-distribution function at the critical point. In the intermediate magnetic-field regime, we find two anomalies in the specific heat. The first anomaly at a temperature T_m is associated with the melting transition of the flux-line lattice. The Lindemann ratio at the melting is given by $c_L \approx 0.24$. The second anomaly at a temperature T_z is one where phase coherence in the BCS order parameter across the sample along the field direction is destroyed. We argue that $T_m = T_z$ in the thermodynamic and continuum limit. Hence, there is no regime where the flux-line lattice melts into a disentangled flux-line liquid. The loss of phase coherence parallel to the magnetic field in the sample is argued to be due to the proliferation of closed non-field-induced vortex loops on the scale of the magnetic length in the problem, resulting in flux-line cutting and recombination. In the flux-line liquid phase, therefore, flux lines appear no longer to be well-defined entities. Above the melting temperature, the system always exhibits an *incoherent vortex-liquid phase* characterized by lack of phase coherence in the BCS order parameter parallel to the magnetic field. For increasing anisotropy, we resolve a δ-function peak in the specific heat. A finite-size scaling analysis of the δ-function peak specific-heat anomaly at the melting transition is used to extract the discontinuity of the entropy at the melting transition. This entropy discontinuity is found to increase rapidly with mass anisotropy, at least for not too layered compounds. [S0163-1829(98)01105-9]

I. INTRODUCTION

A number of recent experiments have reported results of a first-order melting transition of the Abrikosov flux-line lattice (FLL).[1–8] The reported magnitudes of the latent heat have all in general been in surprisingly good agreement with a *prediction* of Hetzel and co-workers for the discontinuity in the entropy at the melting transition based on extensive Monte Carlo simulations of the uniformly frustrated three-dimensional (3D) XY model.[9]

Schilling *et al.* have reported calorimetric measurements on an untwinned $YBa_2Cu_3O_7$ (YBCO) single crystal, in the intermediate field regime $B \in (1-7)$ T, and find a FLL melting transition with a virtually field-independent entropy jump $\Delta S \sim 0.45 k_B$ per vortex per layer.[7] In $Bi_2Sr_2Ca_1Cu_2O_8$ (BSCCO) single crystal at very low magnetic inductions, $B \in (1-375)$ G, it was found that a FLL melting transition occurs with an enormous entropy jump $\Delta S(B=1 \text{ G}) \sim 6 k_B$ per vortex per layer.[4] Furthermore, it was found that $\Delta S(B)$ decreases for increasing B, and vanishes at $B \sim 375$ G.[4] It appears that $\Delta S(B)$ increases dramatically only when $B \to 0$, $T \to T_c$. In fact, it might be argued on the basis of the data of Zeldov *et al.* that $\Delta S(B)$ *diverges* in this limit.

Recently, Tešanović[10] and Nguyen, Sudbø, and Hetzel[11] have proposed an explanation for the inordinately large entropy jump found in Ref. 4. The idea is that the FLL melting

transition takes place at roughly the same temperature as a ''blowout'' of non-field-induced degrees of freedom involving closed vortex loops, resulting in a flux-line liquid phase with considerably larger entropy than what the field-induced vortices alone can provide.

As a step towards understanding these experimental results, we carry out extensive Monte Carlo simulations, together with a finite-size scaling analysis, on the uniformly frustrated anisotropic Villain model, to be defined below. This model will be argued to be appropriate for describing the physics in extreme type-II superconductors such as the high-T_c superconductors. Here, we present a short review of our results.

For the case $B=0$, we find that the Villain model has *one* single second-order phase transition of the 3D XY-type for all anisotropies considered. *The phase transition in zero magnetic field is caused exclusively by a vortex loop ''blowout,''* to be explained below. This is confirmed by a detailed calculation of the distribution function for loops of a given perimeter, as a function of the perimeter, for various temperatures. In the low-temperature regime, this distribution function is an exponentially decreasing function of the perimeter, indicating that there exists a length scale in the problem associated with a typical size of thermally induced *closed* vortex loops in the system. However, in zero magnetic field there exists a temperature scale, which we denote

as T_c, at which the distribution function is an algebraically decreasing function of the perimeter of vortex loops, indicating that there no longer exists a length scale associated with typical sizes of thermally induced closed vortex loops. In this case, such vortex loops exist on *all* length scales in the problem, up to and including the system size.

This means that the system experiences a thermally induced proliferation of unbounded closed vortex loops, a situation for which Onsager coined the term ''vortex-loop blowout''.[13] In zero magnetic field, such a blowout marks the transition from a normal metal to a superconducting state, or vice versa.[10,12] Many years ago, the vortex-loop blowout transition was suggested to occur in the *neutral* superfluid He[4] at the λ transition.[13] The loop transition in He[4] has more recently been reinvestigated by several authors.[14] In the context of *charged* superfluids in *zero magnetic field* a corresponding loop transition was suggested to occur in *isotropic* lattice superconductor models several years ago by Dasgupta and Halperin,[12] and more recently by Korshunov.[15] The suggestion that features of this zero-field transition may survive in finite magnetic fields, and thus be of importance for the statistical mechanics of the *vortex-liquid phase*, has been suggested by Tešanović,[10] and considered recently by us in detailed Monte Carlo simulations of the lattice London model.[11]

The main purpose of the present paper is to study, via detailed Monte Carlo simulations, the fate of the zero-field Onsager-Dasgupta-Halperin transition when a magnetic field is applied to an extreme type-II superconductor, using the somewhat simpler more familiar uniformly frustrated anisotropic Villain model, which is related to the lattice London model via a duality transformation.

For finite fields $B \neq 0$, we find two sharp features in the specific heat and helicity modulus. In addition, we observe what appears to be a crossover at a considerably larger temperature, in agreement with recent simulations.[16,17]

The first sharp feature we find, at a temperature that we denote as T_m, is identified as the first-order melting transition of the FLL. The second sharp feature is more subtle. It takes place at a temperature that we denote as T_z. At the temperature T_z, we find that the phase coherence in the BCS superconducting order parameter across the sample in the direction of the magnetic field is destroyed. We also find, via our computations, that flux-line cutting and the amount of intersecting flux lines dramatically increases at T_z. Consequently, above T_z, phase coherence along the field direction is destroyed. *Furthermore, for the anisotropies considered in this paper, it occurs that $T_z \rightarrow T_m$ from above as the system size is increased. T_z never drops below T_m,* for reasons to be explained below. We emphasize that we at this stage are limiting this statement to the case of *infinite* penetration depth, since the results are obtained within the uniformly frustrated Villain model only.

From this we draw two conclusions. First, when the flux-line lattice melts, it does not melt into a flux-line liquid that has phase coherence along the direction of the applied magnetic field in any temperature regime. This however does not mean that the flux-line liquid is an entangled vortex system: At $T_z \rightarrow T_m$ we find that flux-line cutting and intersectioning of flux lines with closed vortex loops of diameter on the scale of the magnetic length, increases abruptly. Hence,

the flux lines cannot be considered as well defined in the liquid phase. Second, in the present simulations on the anisotropic, uniformly frustrated Villain model, we never observe an entangled flux-line *lattice phase* of the type described by Frey, Nelson, and Fisher[18] for the layered case. However, we cannot access extreme anisotropies in our simulations, for reasons to be explained in Sec. II D, and therefore do not rule out the existence of a ''supersolid phase'' such as proposed in Ref. 18.

We also observe a crossover that takes place at a temperature that marks the onset of strong diamagnetism, not associated with global phase coherence in the superconducting BCS order parameter, but with phase coherence throughout finite domains. It takes place at a temperature well above both T_m and T_z, which we denote as T_{Bc2}. Usually, this crossover is identified with B_{c2}, the upper critical field, and signals the onset of strong diamagnetic fluctuations. This crossover is the remnant of the zero-field second-order phase transition that marks the onset of the transition from metallic to superconducting behavior. The filling fractions we consider in this paper, $f = \frac{1}{32}$ and $f = \frac{1}{72}$, may be converted into a magnetic field of the order of 10 T, which is not particularly low. The present paper, therefore, does not address the issue of how the crossover at B_{c2} in finite large fields evolves into the sharp second-order transition in zero field. This issue is of fundamental importance, and remains open.

The rest of this paper is organized as follows. In Sec. II we describe the uniformly frustrated anisotropic Villain model along with the approximations inherent in this description of a superconductor. We also give the connection between these models and the lattice London model. Then we define the physical quantities to be considered, and their measurements in the simulations. In Secs. III and IV we show and discuss our results for the zero-field case and the finite-field case, respectively. Finally, in Sec. V we summarize our main findings. The derivations of the helicity moduli we consider, both in terms of phase variables and in terms of vorticities, are given in two appendixes.

II. THE MODEL AND DEFINITIONS

A. The model

Our starting point is the anisotropic lattice superconductor model (LSM) (that semantically should be distinguished from the lattice London model),[12,15,19] defined by the partition function

$$Z = \prod_{\mathbf{r}} \prod_{\nu=x,y,z} \left(\int_{-\pi}^{\pi} \frac{d\theta}{2\pi} \sum_{m_\nu=-\infty}^{\infty} \int_{-\infty}^{\infty} dA_\nu \right)$$
$$\times \exp(-H_{\text{LSM}}/k_B T),$$

$$H_{\text{LSM}} = \frac{J_0}{2} \sum_{\mathbf{r}} \sum_{\mu=x,y,z} \left[\alpha_\mu (\nabla_\mu \theta - 2\pi m_\mu - A_\mu)^2 \right.$$
$$\left. + \frac{\lambda_\mu^2}{d^2} (\nabla \times \mathbf{A})_\mu^2 \right]. \quad (1)$$

Here, J_0 is the energy scale for the system. Furthermore, α_μ is the anisotropy parameter along the μ direction, and ∇ denotes a lattice derivative. The variable $\theta(\mathbf{r}) \in [-\pi, \pi)$ is
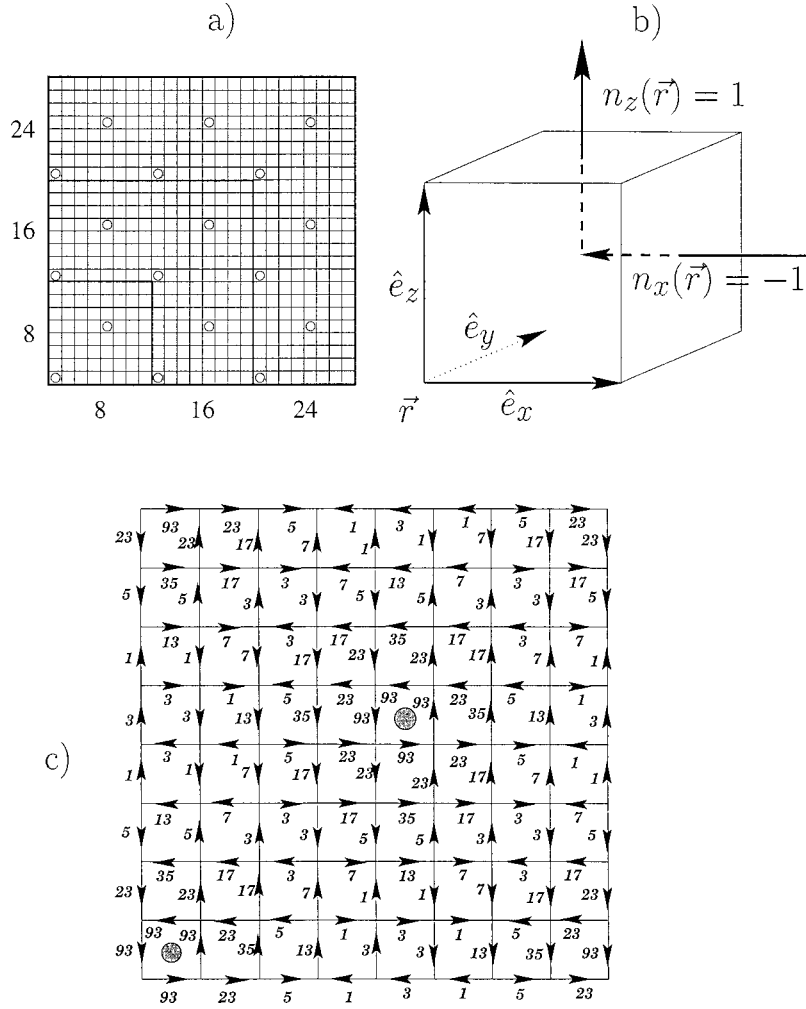
FIG. 1. (a) The ground-state flux-line configuration for $f=1/32$ and system sizes $L=8,16,24$. (b) A cubic unit cell with two elementary vortex segments penetrating two plaquettes of the unit cell. (c) The ground-state current pattern in the ab plane in units of $2\pi/384$ for the 8×8 vortex lattice unit cell. The arrows indicate the direction of the currents on each link. The current pattern in this ground state is complicated, but nevertheless exhibits a high degree of symmetry.

the phase of the complex superconducting order parameter $\Psi(\mathbf{r})$ at site $\mathbf{r}$ of a three-dimensional numerical lattice with lattice constant d, $m_\mu(\mathbf{r})$ are integer variables defined on the directed link between site $\mathbf{r}$ and site $\mathbf{r}+\hat{e}_\mu$, where $\hat{e}_\mu$ is the primitive vectors for the cubic unit cell ($|\hat{e}_\mu|=d$, Fig. 1). The contribution $A_\mu(\mathbf{r})$ to the gauge-invariant phase of the order parameter is related to the vector potential $\mathbf{A}_{vp}(\mathbf{r})$ by

$$A_\mu(\mathbf{r}) \equiv \frac{2\pi}{\Phi_0} \int_{\mathbf{r}}^{\mathbf{r}+\hat{e}_\mu} d\mathbf{r} \cdot \mathbf{A}_{vp}(\mathbf{r}'),$$

where $\Phi_0=2.07\times10^{-15}$ T m^2 is the flux quantum. Finally, λ_μ is the London penetration depth along the μ direction.

In this model, we neglect fluctuations of the amplitude in the complex superconducting order parameter, i.e., $\Psi(\mathbf{r}) = |\Psi(\mathbf{r})|e^{i\theta(\mathbf{r})} \sim \Psi_0 e^{i\theta(\mathbf{r})}$. The lattice London model is obtainable from the lattice superconductor model by explicitly performing the θ and A_μ integrations in Eq. (1), as shown first by Korshunov and more recently by Carneiro.[15,19]

To study the physics of high-T_c superconductors, we consider a three-dimensional *cubic lattice, with linear dimension* Ld, and with a uniaxial anisotropy $\Gamma \equiv \lambda_c/\lambda_a$. In these simulations the applied magnetic field, and hence the net

magnetic induction B, is taken along the crystal $\hat{c}$ axis. Here, λ_a and λ_c are the penetration depths in the crystal ab plane (CuO$_2$ plane) and along the crystal $\hat{c}$ axis, respectively. Subsequently, we will take the limit λ_a, $\lambda_c \rightarrow \infty$, but in such a way that the ratio λ_c/λ_a is maintained constant. We take our coordinate $(\hat{x},\hat{y},\hat{z})$ axis parallel to the crystal $(\hat{a},\hat{b},\hat{c})$ axis, respectively. Periodic boundary conditions in all directions are assumed. The basic parameters of the LSM are given by[19]

$$J_0 = \frac{\Phi_0^2 d}{16\pi^3\lambda_a^2}, \quad \alpha_\mu = \frac{\lambda_a^2}{\lambda_\mu^2}.$$

Here, d may tentatively be interpreted as the distance between two CuO$_2$ layers *in adjacent unit cells*. The vorticities $n_x(\mathbf{r}),n_y(\mathbf{r})$ [corresponding to fundamental vortex-line segments parallel to the ab plane, defined in Eq. (4)] are assumed to exist *in between* CuO$_2$ double or multiple layers in compounds such as YBCO and BSCCO. We use the numerical lattice unit as a measure of the in-plane coherence length, $\xi_a \sim d$. (Note that since the numerical factor relating ξ_a to d is not uniquely determined in our approach, the filling

fraction f does not uniquely determine the magnitude of the applied magnetic field. Variation of f may thus be viewed as a variation of B, but alternatively a reduction of f may be viewed as an improvement of the approximation to the continuum limit at fixed induction B.)

As for the London model, the LSM is appropriate for describing the physics of extreme type-II superconductors ($\lambda_a \gg \xi_a$) in the field regime $B \ll B_{c2}$, where B_{c2} is the upper critical magnetic field, implying $a_v \gg \xi_a$. Thus, spatial variations of the *amplitude* of the superconducting order parameter may be neglected. In these simulations it is also postulated that the penetration length is essentially infinite, which in practice means that they are at least much larger than the average distance between vortex lines, when the field is finite. Hence we also have the requirement $B \gg B_{c1}$. In terms of magnetic induction, our simulations are thus, strictly speaking, limited to the field regime $B_{c1} \ll B \ll B_{c2}$ *when finite fields are considered*. For our zero-field results, the complete suppression of gauge fluctuations implies that the penetration depth of the model must be at least larger than any system sizes considered.

The Monte Carlo simulation time t_{MC} for the LSM on a cubic system with linear dimension L is of order L^6. The suppression of the gauge-field fluctuations, using the limit $\lambda_\mu = \infty$, reduces the required computer time dramatically, t_{MC} to $\sim L^3$. The neglect of gauge fluctuations reduces the LSM to the uniformly frustrated anisotropic Villain model,[14,17,21] which is the model used in this paper. It is defined by the following partition function after performing the sum over $m_\mu(\mathbf{r})$ in Eq. (1) explicitly,

$$Z = \prod_{\mathbf{r}} \left(\int_{-\pi}^{\pi} \frac{d\theta}{2\pi} \right) \exp(-H_v/k_B T),$$

$$H_v = J_0 \sum_{\mathbf{r}} \sum_{\mu=x,y,z} V_\mu(\nabla_\mu \theta - A_\mu; T),$$

$$V_\mu(\chi; T) = -\frac{k_B T}{J_0} \ln \left\{ \sum_{m=-\infty}^{\infty} \exp \left[-\frac{J_0 \alpha_\mu}{2 k_B T} (\chi - 2\pi m)^2 \right] \right\}. \tag{2}$$

The advantage of the Villain model compared to the lattice London model used in earlier large-scale simulations we have performed on the Abrikosov vortex lattice,[11] is that is allows considerably larger system sizes to be studied than with the lattice London model. The latter model has the intuitively appealing feature of allowing simulations on line-like objects, but as we have seen, the Villain model and the lattice London model are in principle equivalent representations of a lattice superconductor model. One other major advantage of the Villain model compared to the lattice London model is that, while it is straightforward to extract unambiguous information about vorticities from the phases of the Villain model, it is impossible to reconstruct unambiguous phase information from the vortex degrees of freedom in the lattice London model. Thus the Villain model straightforwardly provides information on vorticities as well as

phase coherence. Ultimately, the choice of model to use in simulations is dictated exclusively by convenience, and depends to a large degree on what problems to consider. One problem where the lattice London model appears to present clear advantages over the Villain model is the problem of numerical simulations of flux creep in the presence of pinning.

The uniformly frustrated anisotropic Villain model is appropriate for describing the physics of extreme type-II superconductors in the limit where the penetration depth is larger or comparable to the system size (zero magnetic field) or when the penetration depth is much larger than the average distance between flux lines $\lambda \gg a_v$ (finite magnetic fields).

B. The ground state

The current corresponding to the gauge invariance phase differences

$$j_\mu(\mathbf{r}) = \theta(\mathbf{r} + \hat{e}_\mu) - \theta(\mathbf{r}) - A_\mu(\mathbf{r}),$$

is defined on the directed link between site $\mathbf{r}$ and site $\mathbf{r} + \hat{e}_\mu$, $j_\mu(\mathbf{r}) \in [-\pi, \pi)$. This current obeys two conditions: (1) There are no net current sinks or sources in the ground state

$$\sum_{\nu=x,y,z} \nabla_\nu j_\nu(\mathbf{r}) = 0. \tag{3}$$

(2) The counterclockwise line integral of the currents around any plaquette of the numerical lattice with a directed surface normal in the μ direction at site $\mathbf{r}$ *must always* be

$$\sum_{Ci} j_\nu(\mathbf{r}) = 2\pi[n_\mu(\mathbf{r}) - f_\mu]. \tag{4}$$

Here, Ci is the closed path traced out by the links surrounding an arbitrary plaquette, and ν represents the Cartesian components of the current in the directions of the links that comprise the closed path Ci. Furthermore, $n_\mu(\mathbf{r}) = 0, \pm 1$ represents a vortex segment *penetrating the plaquette enclosed by the path Ci*. The situation is illustrated in Fig. 1. Furthermore, f_μ is the filling fraction along the $\hat{\mu}$ direction, defined in Eq. (5). In this way, we can find *the distribution of vortex segments* $\mathbf{n}(\mathbf{r})$, by calculating the counterclockwise line integral of the currents around every plaquette in the system. Hence, the distribution of gauge-invariant current also gives information, essentially by a duality transformation, about the FLL structure function.

To perform a finite-size scaling analysis, we employ the following procedure to find the current pattern in the ground state. Given a density of flux lines $f = \frac{1}{32}$, we design an 8×8 *vortex lattice unit cell*, not to be confused with the unit cell of the numerical lattice. This vortex lattice unit cell has two vortices, Fig. 1. The current pattern (Fig. 1) is found by requiring the currents to obey Eq. (3) on every link and Eq. (4) on every plaquette throughout the vortex lattice unit cell. It is possible to reduce the number of unknown currents by requiring the current pattern to have the same symmetry as the ground-state vortex lattice. Periodic boundary conditions at the boundaries of the vortex lattice unit cell are used. By

repeating the vortex lattice unit cell, we can design the current pattern of all systems with size $m8 \times n8 \times l$, (m,n,l) being positive integers.

The flux-line density along the μ direction is defined as f_μ, and is given by

$$f_\mu = \frac{\Sigma_\mathbf{r} n_\mu(\mathbf{r})}{L^3}. \tag{5}$$

In the ground state, a uniform magnetic induction along the crystal $\hat{c}$ axis $\mathbf{B} = B\hat{z}$ gives a periodic structure of straight flux lines aligned with $\mathbf{B}$ with hexagonal symmetry on a continuum substrate ab plane, the well-known hexagonal Abrikosov vortex lattice. In terms of the above densities f_μ this is expressed as

$$f_z = \frac{Bd^2}{\Phi_0} \equiv f, \quad f_x = f_y = 0.$$

In our simulations, it is not possible to exactly load the hexagonal Abrikosov vortex lattice onto our numerical mesh, which we have chosen to be square. This means that the underlying numerical mesh necessarily introduces a distortion of the hexagonal ground state. The numerical mesh represents a commensuration potential that acts as a perturbation on the ground state, and tends to ''freeze'' the flux lines into a structure commensurate with it. The flux lines will however tear themselves off such a commensuration potential caused by the numerical lattice at a high enough temperature, which we denote a ''depinning'' temperature T_{dp}. Note that this depinning temperature has nothing to do with a real pinning potential, it is purely an artifact of the underlying numerical lattice. In the continuum limit, it would be zero. It is at present unclear to what extent the numerical mesh represents a singular perturbation on the continuum limit in a 3D system. The well-known results of Nelson and Halperin[24] and Young[25] concerning the effects of periodic commensuration potentials in 2D, indicates that if the filling fraction is small enough in 2D, T_{dp} will be smaller than any other relevant energy scale in the problem. This has also been nicely confirmed in a number of recent simulations on 2D systems.[26] Note that, by using a square numerical mesh, we counteract the disadvantage of the distortion of the hexagonal lattice by a reduction in the strong commensuration effects we would have encountered if we had chosen a triangular numerical mesh, which admits an exact hexagonal lattice ground state.

By using low enough filling fractions f_z, it may be hoped even in 3D to achieve a satisfactory approximation to the continuum limit. That is, we hope that the depinning temperature T_{dp}, which appears purely as an artifact of defining the model on a numerical lattice, drops below all other relevant temperatures in the problem, including the putative melting temperature T_m of the FLL.

That such a thermal depinning from the numerical lattice can actually be achieved in higher dimensions than 2D is by no means clear, since commensuration effects are much more pronounced in 3D than in 2D. In fact, in the thermodynamic limit, thermal depinning from the numerical lattice, strictly speaking, *cannot* happen in 3D. Therefore, in order to mimic the statistical mechanics of the FLL defined on a con-

tinuum substrate in 3D, one carefully has to choose sample geometry in simulations as follows: It is crucial to have a sample geometry where the distance between flux lines is tailored to suit the thickness of the sample in such a way that the commensuration potential along the direction of the flux lines does not cause pinning to the numerical lattice at the temperatures of interest. This implies that simulations must be carried out on relatively flat slabs. Simulations on ''tower''-shaped slabs[17] are probably not able to capture the continuum limit. In our simulations, we have checked that in fact such a depinning transition from the numerical mesh takes place at a temperature T_{dp}^{3D}, which is below the temperatures of primary interest. Hence, in our simulations the continuum limit ought to be adequately mimicked. Note that for filling fractions $f = \frac{1}{8}$ and $f = \frac{1}{15}$, the continuum limit is not mimicked satisfactorily. In these cases, it is clear that pinning to the numerical mesh strongly influences the results. In this paper, we consider mainly the case of $f = 0$ and $f = \frac{1}{32}$, while some results are also obtained for $f = \frac{1}{72}$.

C. The Monte Carlo simulation

The statistical mechanics of the Villain model of an extreme type-II superconductor is investigated by employing the following Monte Carlo procedure on numerical cubic lattices with linear dimensions $L \in [8,16,24,32,40,48,64,80,96]$. Identical sets of current patterns are loaded onto each layer of the numerical lattice. For the filling fraction $f = \frac{1}{32}$, this current pattern is illustrated in Fig. 1. We update the system, heating the system from the ground state consisting of fL^2 straight field-induced flux lines. A site of the numerical lattice is chosen randomly, and an attempt is made to change the phase on that site with a random amount $\Delta\theta \in [-\pi, \pi)$. The phase change is accepted or rejected according to the standard Metropolis algorithm.

If the accepted phase change causes the current on a link $j_\mu(\mathbf{r})$ to fall outside the range $j_\mu(\mathbf{r}) \in [-\pi, \pi)$, we add an amount $\pm 2\pi$ to the current, such that $j_\mu(\mathbf{r})$ is brought back into the primary interval $j_\mu(\mathbf{r}) \in [-\pi, \pi)$. An important point is that this operation can only generate a closed unit vortex loop around the link where the current is changed, thereby conserving the net induction of the system. No net vorticity is ever introduced by the procedure, and the procedure also guarantees that no flux line can start or end within the sample. It is also important to note that the Monte Carlo procedure described above satisfies detailed balance. Hence, the entire phase space of the Villain model is guaranteed to be exhausted provided the simulations are run for a long enough time. Another point is that the above procedure for limiting the currents to the primary interval also limits the number of vortex segments penetrating a plaquette to at most one per plaquette. In this way, the Villain model differs from the lattice London model, where the number of vortices penetrating each plaquette can be arbitrary. This difference however only becomes important in the high-temperature regime.

The Monte Carlo procedure really updates the gauge-invariant phase differences, or currents $j_\mu(\mathbf{r})$. The simulations are therefore carried out in a manifestly gauge-invariant manner. One Monte Carlo sweep consists of L^3 attempts to change the phases $\theta(\mathbf{r})$ on L^3 randomly chosen sites throughout the lattice. Thus, by such a move we simultaneously change the gauge-invariant phase differences on the six links associated with the relevant lattice point. Each data point for

the quantities we consider is obtained after discarding the first 100 000 (30 000) sweeps for equilibration. The subsequent 400 000 (70 000) sweeps are used to obtain averages. The numbers in parentheses represent the number of sweeps we have for the case of $\Gamma = 1$. To ensure that measurements are independent of each other, we do one measurement per 100 sweeps.

D. Anisotropy and finite-size effects

For $B = 0$ and isotropic couplings, the LSM, the XY model, and the Villain model all have one single phase transition at $k_B T_c / J_0 \simeq 3.0$. The transition is characterized by stiffness in the phase of the superconducting order parameter being lost across the system in all directions, due to a blowout of thermally excited closed vortex loops.

For the anisotropic case, the bare coupling between planes $J_\perp$ in the Villain model is smaller than the in-plane coupling $J_\parallel$. Thus, in the very anisotropic case, the excitation energy of a unit vortex loop parallel to the ab plane is much smaller than the excitation energy for a unit vortex loop containing segments perpendicular to the ab plane.[20] One would naively then expect that thermal excitation of vortex loop parallel to the ab planes would occur at correspondingly lower temperatures than those for which vertical loops appear. This is true for unit vortex loops, but such loops are unimportant for critical behavior. From the point of view of considering $B = 0$ critical phenomena, the important issue is how the anisotropy affects large vortex loops, including vortex loops of order the system size. This is an issue to which we now briefly turn. It is convenient to carry out this discussion in terms of the phases of the superconducting order parameter, rather than in terms of vorticities.

When the temperature approaches the Kosterlitz-Thouless (KT) temperature from above in a quasi-2D system, the phase-coherence length gradually grows. In a strictly 2D system, it would diverge precisely at the KT transition. However, as long as a small coupling between planes exists, no matter how small, then as the KT transition is approached from above, increasingly larger domains of correlated phases are coupled together by the interplane coupling. This strongly renormalizes the bare interplane coupling constant $J_\perp$.[15,22] Hence, the system is isotropized close to, but above, the KT transition, and the transition retains a 3D character. Thus, even an extremely anisotropic system exhibits, precisely as in the isotropic case, one single 3D phase transition. No decoupling transition as proposed in Ref. 23 exists in zero magnetic field.

In simulations on finite systems, care must be taken to ensure that this physics is captured correctly. When the an-

isotropy of the system is increased such that the bare interplane coupling is reduced, one must make sure that the dimensions of the system in the directions parallel to the ab planes are large enough to allow the required renormalization of the coupling constants to run its course without being cutoff prematurely by the system size. Equivalently, one may rescale the size of the system in the z direction, by the factor $1/\Gamma$. Thus, the transverse system size must be tailored to the anisotropy of the system in such a way that critical behavior we study takes place at a *lower* temperature than the energy scale $k_B T^*$ set by

$$k_B T' = \left(\frac{\xi}{d}\right)^2 J_\perp .$$

Here, $J_\perp$ is the bare interplane coupling in the Villain model, and ξ is the coherence length of the phase of the superconducting order parameter at the relevant temperature. If the system is too small in the transverse direction, the renormalization of the bare coupling is cut off by the system size

$$T^* = L^2 J_\perp .$$

Hence, for a given L, we may choose an anisotropy such that $J_\perp$ is so small that T^* becomes smaller than the actual temperature of the 3D critical phenomenon of interest, namely, the vortex-loop blowout. We would then observe a decoupling of planes due to a proliferation of vortex loops in the ab plane that would be unphysical.

This finite-size effect limits the anisotropies we can study consistently, at least in zero magnetic field. In zero field, we find ourselves limited to anisotropies of $\Gamma \lesssim 4$.

A final technical point is that, although a finite magnetic field *a priori* allows larger anisotropies to be studied, the Villain potential itself becomes virtually featureless as a function of its arguments χ, Eq. (2), for large anisotropies. Hence, simulations become impossible to perform meaningfully.

E. The helicity modulus

To probe the global phase coherence in the BCS superconducting order parameter across the entire system, we consider the helicity modulus Υ_μ, defined as the second derivative of the free energy with respect to a phase twist in the μ direction.[17] It basically measures the stiffness of the system to a twist in the phase of the order parameter. In the anisotropic case we have the following generalization of previously obtained expressions for the helicity modulus for isotropic superconductors:[17]

$$\Upsilon_\mu = \frac{J_0^2}{L^3 k_B T} \left\langle \sum_{\mathbf{r},\nu} V_\nu'[\theta(\mathbf{r}+\hat{e}_\nu) - \theta(\mathbf{r}) - A_\nu(\mathbf{r})](\hat{e}_\nu \cdot \hat{e}_\mu) \right\rangle^2 - \frac{J_0^2}{L^3 k_B T} \left\langle \left(\sum_{\mathbf{r},\nu} V_\nu'[\theta(\mathbf{r}+\hat{e}_\nu) - \theta(\mathbf{r}) - A_\nu(\mathbf{r})](\hat{e}_\nu \cdot \hat{e}_\mu) \right)^2 \right\rangle$$

$$+ \frac{J_0}{L^3} \left\langle \sum_{\mathbf{r},\nu} V_\nu''[\theta(\mathbf{r}+\hat{e}_\nu) - \theta(\mathbf{r}) - A_\nu(\mathbf{r})](\hat{e}_\nu \cdot \hat{e}_\mu)^2 \right\rangle . \quad (6)$$

For the details on the derivation of this expression, and a corresponding one in terms of vorticities, see Appendixes A and B. Here, V'_μ and V''_μ are the first and second derivatives, respectively, of the anisotropic Villain potential V_μ defined in Eq. (2). For temperatures $T < T_\mu$ such that $\Upsilon_\mu > 0$, there is phase coherence across the entire system in the μ direction. Hence, the system can sustain a supercurrent in the μ direction. At the temperature $T = T_\mu$ and above, such that $\Upsilon_\mu = 0$, phase coherence along the μ direction is lost. Hence, the vanishing of Υ_μ signals the superconducting–normal-metal transition in the μ direction with the transition temperature T_μ. For the case of finite magnetic induction along $\hat{z}$ axis in the continuum limit, Υ_x and Υ_y should vanish at all temperatures,[27] since a current in the ab plane would exert a Lorentz force on the unpinned flux lines, moving them and thus dissipate energy. When the model is discretized by introducing the numerical lattice, a finite energy for moving them in a direction perpendicular to the $\hat{z}$ direction is also introduced. The existence of a smallest energy to required move flux lines acts as an artificial pinning potential on the FLL, causing T_x ($T_y = T_x$) to be finite. Thus, the FLL ''depins'' from the underlying discrete lattice at a finite temperature $T_x = T_y > 0$. In the continuum limit, as long as no physical pinning of the flux lines is present, we would have $T_x = T_y = 0$, and the flux lines are unpinned at all temperatures. To ensure that the above artificially introduced pinning potential caused by the numerical lattice does not affect the FLL melting transition and any other genuine phase transition we might want to consider, we should consider systems with T_m significantly higher than T_x. The way to achieve this is to consider low enough filling fractions $f = f_z$ of flux lines. Several authors[11,26] have in fact found that T_x decreases for decreasing flux lines density f, and falls below T_m for $f < f_c \simeq \frac{1}{32}$.

F. Vortex-loop distribution

As mentioned in the Introduction, in the LSM, Villain model, and lattice London model, the zero-field normal–metal-superconductor transition corresponds to a vortex-loop blowout analogous to what has long been suggested to occur in the neutral superfluid He^4. To study the blowout of a closed vortex loop in extreme type-II superconductors, we consider the quantity $D(p)$, which we denote the vortex-loop distribution function, and which is given as statistical average of the total number of closed *non-field-induced* vortex loops with a given perimeter p, in our case normalized by the volume of the systems we consider. The following procedure is employed to compute $D(p)$.

We start from an arbitrarily chosen unit cell containing at least one *outgoing* vortex segment penetrating a plaquette of that unit cell. We then follow the direction of this vortex segment *into* the neighboring unit cell. If there is more than one vortex segment leaving the unit cell, one of them is chosen randomly. We continue tracing the path of vortex segments until the path closes upon itself. When the path has closed upon itself, we measure the length l of the path, as well as the net vorticity v_z along $\hat{z}$ axis of the path. Also, we remove the vortex segments along the path to prevent double counting of paths. Because of the periodic boundary condi-

tions, such closed paths of vortex segments can either belong to a field-induced flux line or a non-field-induced closed vortex loop.

In the quantity $D(p)$, we do *not* include the closed paths associated with field-induced flux lines that close on themselves merely due to periodic boundary conditions in the $\hat{z}$ direction. Field-induced flux lines are characterized by a net vorticity in the $\hat{z}$ direction, $v_z \neq 0$. For the purposes of studying the loop transition, we are exclusively interested in closed paths associated with *non-field-induced* vortex loops that physically close on themselves regardless of boundary conditions. Hence, the relevant closed paths of vortex segments are closed vortex loops with perimeter $p = l$ that have net vorticity $v_\mu = 0$ in all directions.

The procedure for tracing out the relevant closed loops is repeated until all nonfield vortex segments in the system have been counted. For $B \neq 0$, this procedure uniquely separates thermally excited closed vortex loops from the field-induced flux lines.

In the low-temperature regime, $D(p)$ depends on the excitation energy $E(p) \sim \varepsilon p$ of the vortex loops with perimeter p, with a Boltzmann factor,[17]

$$D(p) \sim \exp\left(-\frac{\varepsilon p}{k_B T} \right) \sim \exp\left(-\frac{p}{L_0} \right),$$

where ε is a constant representing a line tension, and $L_0 \sim k_B T/\varepsilon$ is a typical perimeter of closed vortex loops present at a given temperature *in the low-temperature regime*. As we will see below, such low-temperature ''confined'' vortex loops may be coarse grained away and are unimportant for the statistical mechanics of the mixed state of an extreme type-II superconductor. In this thermally activated regime, large vortex loops are exponentially suppressed. On the other hand, at the critical point, vortex loops with all perimeters are present. This leads to an algebraic decay of the loop-distribution function vs loop perimeter at the critical point, $D(p) \sim p^{-\alpha}$, where α is an exponent not to be confused with the critical exponent of the specific heat. Hence, monitoring the temperature where $D(p)$ changes its characteristic behavior from exponential decay to algebraic decay, is a way of determining the vortex-loop unbinding temperature.

If we assume that the vortex-loop distribution function scales with the vortex-loop perimeter as some power law, and furthermore assume that the perimeter scales with the vortex-loop radius r, then we have

$$D(r) \sim r^{-\alpha}.$$

We now use a critical scaling analysis to determine α in our case. The assumption is that the loop transition in zero field represents a critical point. If we can then fit numerically obtained exponents at the putative critical point to the scaling results, this would provide further support for the assertion that the loop blowout is responsible for destroying superconductivity in extreme type-II superconductors.

The Villain-model is dual to a 3D Coulomb gas, and the vortex loops are analogous to the vortex-antivortex pairs of the 2D Coulomb gas. We may determine the contribution to the dielectric constant of the 3D Coulomb gas that such loops give. Since the dielectric constant may be related to the

inverse superfluid stiffness, whose scaling dimension is well known on general grounds, we may determine α at the critical point.

The ''dipole-moment'' $P(r)$ of a vortex loop scales with $r^{d-2} \cdot r$, where the charge $\sim r^{d-2}$, and the dipole vector $\sim r$. The contribution to the dielectric constant, or the electric susceptibility, coming from thermally induced loops of size between r is given by[28]

$$\chi_e(r) \sim \varepsilon(r) \sim \frac{\partial}{\partial E} \langle r^{d-1} \cos(\phi) \rangle \Big|_{E=0},$$

where the average should be a thermal average with the Boltzmann factor

$$\exp[-U(r)/k_B T] \sim D(r)\exp[r^{d-1}E \cos(\phi)/k_B T].$$

Here E is an electric field polarizing the medium via the ''charge-loops'' of the 3D Coulomb gas, and ϕ is the angle between the orientation of loops and the applied electric field polarizing the medium. We find

$$\varepsilon(r) \sim r^{2(d-1)-\alpha}.$$

On the other hand, in the superconductor, the superfluid stiffness ρ_s is given by the transverse susceptibility $\chi^\perp \sim G \sim \rho_s$, where G is given by the order-parameter Green's function, $G \sim r^{2-d-\eta}$, and where η is the anomalous scaling dimension of the Green's function appearing due to critical fluctuations, for the 3D XY model we have $\eta = 0.033(4)$. Now we use the fact that $\varepsilon \sim \rho_s^{-1}$, to find

$$2(d-1) - \alpha = d + \eta - 2,$$

$$\alpha = d - \eta.$$

In our case, we may evaluate the loop-distribution function at the anomalous peak in the specific heat, and fit the result to a power law with the exponent 3, obtained by assuming critical scaling. We will see below that the fit is excellent, lending further support to the assertion that in zero field, the superconductor–normal-metal phase transition in an extreme type-II superconductor is due to a vortex-loop blowout transition.

It is also interesting to note that another way of estimating the relevance of closed vortex loops, is to see whether they can be coarse grained away or not. A rough criterion for coarse graining them away, would be that the loop distribution integrated over the volume of the system should be finite, i.e.,

$$\int d^d r D(r) \sim \int_0^\Lambda dr\, r^{d-1-\alpha} \sim \Lambda^{d-\alpha}.$$

Thus, loops may be coarse grained away provided that $\alpha > d$. In the low-temperature regime, we have seen that the loops are even exponentially suppressed, and certainly satisfy this criterion. The marginal case $\alpha = d$ gives an integrated distribution $\sim \ln\Lambda$. However, at the critical point, $\alpha = d - \eta$ is less than the required value for coarse graining, furthermore critical fluctuations as manifested by a nonzero positive value of the exponent η, will increase the relevance of vortex loops, as expected.

G. Specific heat

In addition to indirect measurements of the latent heat of melting, such as measured by local magnetization measurements on BSCCO,[4] direct calorimetric measurements of the specific heat are also useful for estimating the latent heat of the melting transition of the FLL, or any other phase transition the vortex system might suffer. Such measurements are now available[7] both in zero field and in finite field. In Ref. 29, the specific-heat anomaly in a twinned YBCO sample is measured systematically with varying magnetic field. It evolves smoothly from the zero-field result as the magnetic field is increased. Moreover, the integrated anomaly appears to be approximately constant as the magnetic field increases. This raises the question of what sort of phase transition, if any, the specific-heat anomaly in finite magnetic fields should be associated with. Due to its smooth evolution from the zero-field case, it appears rather unlikely that this sizeable anomaly has anything whatsoever to do with FLL melting. Rather, it seems to suggest that there are remnants of the zero-field transition, which we will describe in detail below, at finite magnetic fields.

We may investigate this issue, by calculating the specific heat of the Villain model, and correlate the specific-heat anomalies with the temperature dependence of the structure function $S(\mathbf{K})$ as well as with the phase stiffness Υ_z. Thus we should in principle be able to decide whether or not the major features in the specific heat have anything to do with FLL melting or vortex-loop blowout, also at finite fields. In zero field, we will be able to precisely correlate, for all anisotropies, the anomaly in the specific heat with the vortex-loop blowout transition. In a finite field, the situation is considerably more complicated. We find three anomalous features in the specific heat. The major feature in the specific heat, the remnant of the zero-field transition, occurs at temperatures well above those where the structure function of the FLL, and the phase stiffness across the sample along the field direction, vanishes.

To calculate the specific heat per site C, we use the usual fluctuation formula

$$\frac{C}{k_B} = \frac{1}{L^3} \frac{\langle H_v^2 \rangle - \langle H_v \rangle^2}{(k_B T)^2}.$$

The Villain model has a rather unusual property in that the Boltzmann factor appearing in the partition function $\exp(-H/k_B T)$ involves an explicitly temperature-dependent Hamiltonian, Eq. (2). The usual fluctuation formula for the specific heat is valid, strictly speaking only if H is temperature-independent. Nevertheless, we will use the above standard expression for calculating the specific heat for convenience, and neglect the extra terms that should be included from the explicit temperature dependence of the Villain potential, Eq. (2). We have checked the validity of this approximation by comparing the thus obtained specific heat per site C with the alternative standard method of extracting the specific heat per site C from its basic definition in terms of the internal energy of the system

$$\frac{C}{k_B} = \frac{1}{L^3} \frac{\partial \langle H_v \rangle}{\partial (k_B T)}.$$

We find that these two ways of calculating the specific heat differs only in the very high-temperature regime, outside the temperature range of interest in this paper.

H. The structure function

To probe the FLL melting, we consider the structure function for n_z vortex segments, i.e., vortex segments directed along the average induction. The structure function $S(\mathbf{k})$ is defined by[11,30]

$$S(\mathbf{k}) = \frac{\langle |\Sigma_{\mathbf{r}} n_z(\mathbf{r}) \exp[i\mathbf{k}\cdot\mathbf{r}]|^2 \rangle}{(fL^3)^2}.$$

For our ground state with the flux lines density $f = \frac{1}{32}$ (Fig. 1), the unit reciprocal lattice vectors for the FLL are

$$\mathbf{K}_1 = 2\pi[\tfrac{1}{8}, -\tfrac{1}{8}], \quad \mathbf{K}_2 = 2\pi[0, \tfrac{1}{4}].$$

In the FLL phase, $S(\mathbf{k}_\perp, k_z = 0)$ has δ-function Bragg peaks at $\mathbf{k}_\perp = \mathbf{K}(m,n) = m\mathbf{K}_1 + n\mathbf{K}_2$ $(m,n=0,\pm 1,\pm 2,\pm 3,\dots)$. The vectors $\mathbf{K}$ are located within the first Brillouin zone. When the FLL melts, the Bragg peaks are smeared out. The lowest temperature T, where $S(\mathbf{K}, k_z = 0)$ vanishes, thus defines the FLL melting temperature T_m. For simplicity, we consider only the structure function $S(\mathbf{Q} \equiv S(\mathbf{K}_2, k_z = 0))$.

I. Flux-line cutting and intersection

The issue of flux-line cutting and flux line and entanglement, as well as the suggested possible resulting vortex states originating from the latter, such as the analogs of 2D Bose superfluids and supersolids, and even topological vortex glass states, have been issues of considerable controversy over the last ten years. In particular, the effect of entanglement on the FLL melting transition and the statistical mechanics of the FLL, has received considerable attention.

In principle, flux-line entanglement could be responsible for the drop in Υ_z we observe at the temperature T_z. It is of interest to correlate the amount of "close vortex-line encounters" with the anomalies we obtain in the specific heat. This will allow us to at least tentatively decide whether or not flux lines start to intersect or cut at any of the temperatures T_m, T_z, or T_{Bc2}.

Intersection and cutting of flux lines tend to act as efficient modes of *disentanglement* of flux lines. It is unlikely that a flux-line liquid phase that suffers large amounts of thermally induced collisions between flux-line segments, which in turn strongly indicates that flux-line cutting takes place, can also sustain heavily entangled vortex configurations. Hence, if we can show that the amount of close vortex-segment encounters is substantial at the temperature where Υ_z goes to zero, we may at least tentatively conclude that the drop in Υ_z is *not* due to entanglement of flux lines.

To study the intersection and or cutting of flux lines, we define a parameter ρ, which is a measure of the amount of flux-line cutting and intersection that takes place in the flux-line liquid.

$$\rho \equiv \frac{N_{\text{int}}}{N_\phi}, \tag{7}$$

where N_{int} is the total number of unit cells having 4 or 6 vortex segments penetrating their plaquette, and N_ϕ is the number of field-induced flux lines in the system. Note that with this definition, we only consider ρ for the case of finite fields. This quantity gives us some intuition on how well defined we may expect individual field-induced flux lines to be in the liquid phase.

In the Villain model, each plaquette can carry at most one vortex segment. This is because the vorticities are defined in terms of gauge-invariant phase differences, defined on the interval $j_\mu(\mathbf{r}) \in [-\pi, \pi]$. The distribution of vortex segments $\mathbf{n}(\mathbf{r})$ has no divergence $(\Sigma_{\mu=x,y,z} \nabla_\mu n_\mu(\mathbf{r}) = 0)$. Thus, a single unit cell can only carry 0, 2, 4, or 6 vortex elements. If a unit has more than 2 plaquettes that are pierced by vortex segments, then that corresponds to one of the three following situations: (1) an intersection between two different flux lines; or (2) an intersection between a flux line and a closed vortex loop; or (3) an intersection between two different closed vortex loops.

Inside a unit cell, it is impossible to decide which possibility is realized. In principle, ρ as defined above counts all of these possibilities, while flux-line intersection and flux-line cutting correspond to case (1).

III. RESULTS, ZERO MAGNETIC FIELD

We now present the results of our Monte Carlo simulations, and consider first the case of zero magnetic induction $\mathbf{B} = 0$. From now on we measure the *specific heat per site C in units of* k_B, *the helicity moduli* Υ_x *in units of* J_0, Υ_z *in units of* J_0/Γ^2, *and the temperature T in units of* J_0/k_B.

Two values of $\Gamma = \lambda_c/\lambda_a$, the anisotropy parameter, are considered: $\Gamma = 1$ and $\Gamma = 3$. We will present results for the quantities relevant to the zero-field case, namely, the helicity modulus, the vortex-loop distribution function, and the specific heat. An important point is that we need to, in the zero-field case, to be able to correlate the temperature at which the helicity modulus Υ_z vanishes, with the temperature at which the loop-distribution function $D(p)$ qualitatively changes behavior from an exponential dependence on the loop perimeters to algebraic dependence on the loop perimeters. Moreover, both these features must be correlated with the temperature where an anomaly in the specific heat is found, as discussed in Sec. II D. For arbitrary anisotropy Γ, the system should only have one single phase transition, the normal–metal-superconductor transition.

A. Helicity modulus

The results for the helicity modulus Υ_μ, Eq. (6), in zero magnetic field and in the isotropic case $\Gamma = 1$, are shown in Fig. 2. We have confirmed that all moduli $\Upsilon_x, \Upsilon_y, \Upsilon_z$, are equal in this case, and therefore only exhibit Υ_z. The results are shown for the system sizes $L = 8, 32, 64, 96$. Note that the drop in Υ_z becomes sharper as the system size increases, and the value of T where Υ_z appears to vanish, becomes smaller. When $\lambda \to \infty$, Υ_z, which is the stiffness of the phase of the superconducting order parameter to a twist, is proportional to the superfluid density ρ_s. (For a finite λ this identification no longer holds, as emphasized in Ref. 27.) We have found from the numerics that $\Upsilon_z \sim |T - T_c|^{2/3}$, consistent with the
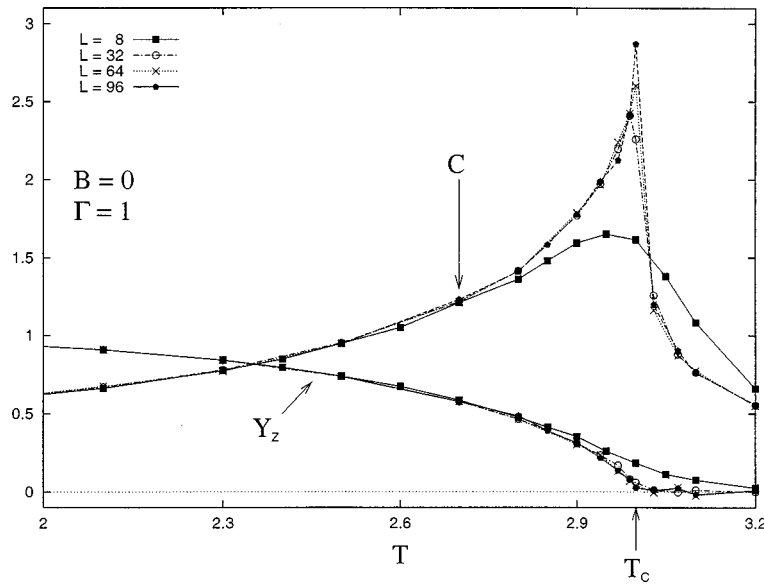
FIG. 2. Helicity modulus Y_z and the specific heat per site C vs temperature, for $B=0$, $\Gamma=1$ (isotropic) and system sizes L $=8,32,64,96$.

Josephson scaling relation, $\rho_s \approx |T-T_c|^\nu$, where ν is the correlation length exponent $\nu=2/d=\frac{2}{3}$. Due to the identification $Y_z \sim \rho_s$, we conclude that the vanishing of the helicity modulus corresponds to the normal–metal-superconductor transition. The transition occurs at the temperature $T=3.0$ in units of J_0/k_B.

The results for the helicity modulus in the anisotropic case $\Gamma=3$ are shown in Fig. 3. The situation at first glance appears considerably more complicated than in the isotropic case, despite our expectations that the physics basically should be the same as in the isotropic case, cf. our discussion in Sec. II D. A striking feature is that for $\Gamma=3$, the helicity modulus Y_z appears to vanish distinctly below the tempera-

tures at which the helicity moduli Y_x, Y_y vanish. (Y_x and Y_y turn out identical in all our simulations, and we therefore only exhibit Y_x.) Note however that there is an important finite-size effect in the results: As L increases, Y_x vanishes at progressively lower temperatures while Y_z vanishes at progressively higher temperatures. As L increases, Y_z and Y_x appear to approach zero at the *same temperature*. Due to the limitations in available system sizes, we have not been able to perform the simulations at higher anisotropies than $\Gamma=3$ *for the zero-field case*. At lower anisotropies $1<\Gamma<3$, the same finite-size effect as described above is seen. For lower values of the anisotropy it is also more obvious that the two temperatures at which Y_z and Y_x vanish, ap-
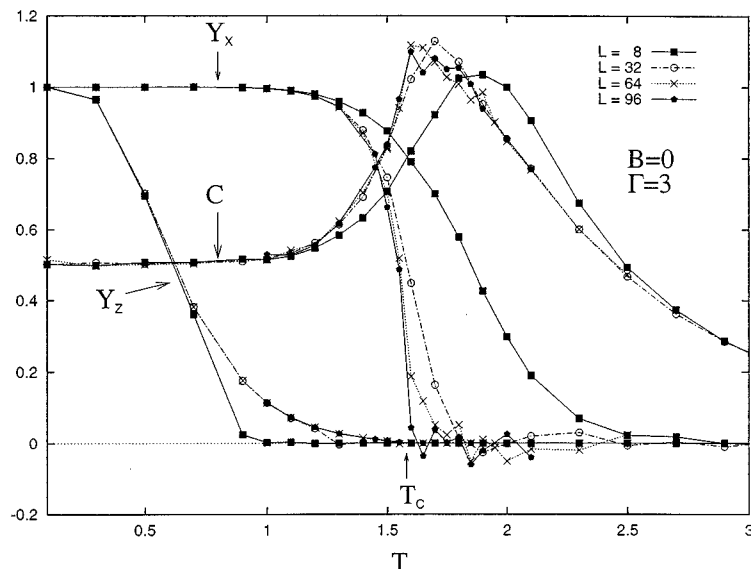
FIG. 3. Helicity moduli Y_x, Y_z, and the specific heat per site C vs temperature, for $B=0$, $\Gamma=3$, and system sizes $L=8,32,64,96$. For increasing system size L, T_x approaches $T_c=1.57$ from above, and T_z increases approaching T_c from below. The layered system has only one phase transition.
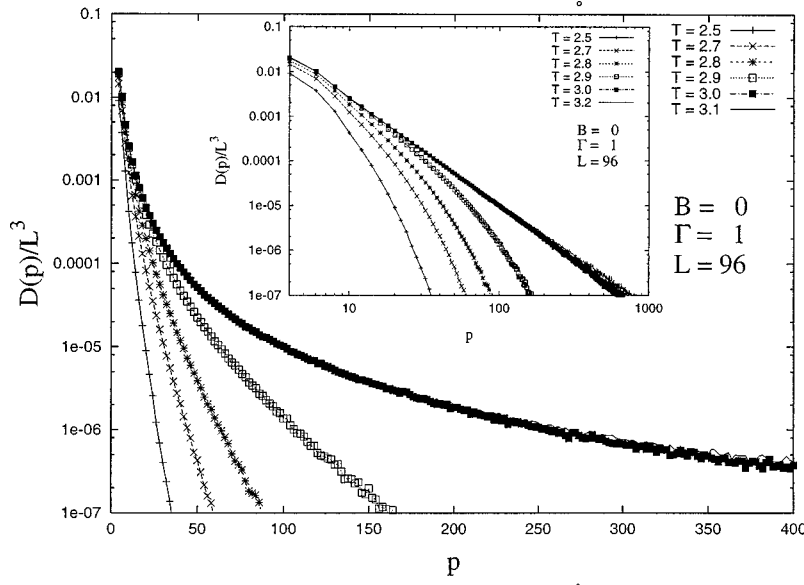
FIG. 4. The distribution function $D(p)/L^3$ of thermally excited, non-field-induced, closed vortex loops per site as a function of perimeter p, for $B=0$, $\Gamma=1$, $L=96$, and various temperatures. It has been normalized this way to facilitate comparison between different system sizes. For $T<T_c\simeq3.0$, $D(p)$ is best fit to an exponential decay. For $T=T_c$, $D(p)$ is best fit to an algebraic decay $D(p)\sim p^{-\alpha}$ with exponent $\alpha=3$ excellently, indicating an Onsager loop-transition at $T=T_c$. The inset shows $D(p)$ on a log-log plot. The slope of the straight line, obtained at $T=T_c$, is -3. At $T<T_c$ the curves show a marked downward curvature, indicating a faster-than-algebraic decay of $D(p)$. This point is discussed in Sec. II F.

proach each other with increasing system size L. For the anisotropic case $\Gamma=3$, the transition occurs at $T=1.57$ in units of J_0/k_B.

B. Loop distribution

In order investigate the excitations responsible for destroying the superconducting phase coherence and the superfluid stiffness as evidenced by our results for Y_z, we probe the amount of closed vortex loops that are thermally excited in the superconductor model at the temperature where Y_z vanishes. We first discuss the isotropic case $\Gamma=1$.

The results for $D(p)$ are shown in Fig. 4, for the largest system we have considered, $L=96$. The figure shows $D(p)$ as a function of the loop perimeters p, for various temperatures in the range $T\in[2.3,3.3]$. Recall from above that in the isotropic case, the helicity modulus vanished at $T\approx3.0$. From Fig. 4, particularly from the inset of this figure, we observe a qualitative change in $D(p)$ precisely at the temperature $T=3.0$. The inset shows the distribution function on a log-log plot, and it is seen that the decay is faster-than-algebraic for $T<T_c$ while it is a precise power law with exponent α in good agreement with a scaling analysis assuming that the vortex-loop blowout is a critical point. We attribute the slight deviation in the exponent α between the simulations and the theory as due to the presence of vortex loops of more complicated shapes, such that the circumference of the loops do not all scale with their diameter. We have tentatively suggested an exponential decay in the low-temperature phase, but this is not unambiguous. However, our main point is that for $T<T_c$ the decay cannot be a power law, while at $T=T_c$, the power law we find is precisely the same as the one we predict analytically assuming that the vortex-loop blowout is in fact a critical point.

Hence, based on the above, we conclude that at $T=3.0$, a sharp phase transition occurs from a low-temperature phase where closed vortex loops are confined to some typical size $L_0(T)$, to a high-temperature phase where closed vortex loops of all sizes up to and including the system size, exists. Thus, in the isotropic case we have been able to precisely correlate the drop in Y_z with a vortex-loop blowout, and from the previous paragraph we must identify this as the superconductor–normal-metal transition.

The loop-distribution function for the anisotropic case $\Gamma=3$ is shown in Fig. 5. Due to the drop in the critical temperature of the system, we now show $D(p)$ as a function of p for temperatures in the range $T\in[0.7,2.1]$. Again, we observe a qualitative change in the behavior of $D(p)$ from exponential decay to algebraic decay, at a temperature $T\approx1.6$, which correlates almost perfectly with the temperature $T=1.57$ at which the helicity moduli Y_z and Y_x vanish for $\Gamma=3$. If we fit $D(p)\sim p^{-\alpha}$ at this temperature, we again find the exponent $\alpha=3$, as in the isotropic case.

So far, our expectations based on the discussion in Sec. II D are borne out. To illustrate the point further, in the inset of Fig. 5, we show the distribution function $D(p)$ for $\Gamma=3$ and the same range of temperatures, for the smaller system $L=16$. The important difference between these two cases is that for $L=16$, algebraic decay of $D(p)$ appears to persist down to lower temperatures than for $L=96$. For larger systems the vortex-loop blowout is suppressed due to the fact that the interplane coupling is allowed to renormalize further without being cutoff by a small system size. Hence, what appeared to be a separate vortex-loop blowout at a low temperature $T=1.1$ for $L=16$, has been pushed up to the correct temperature $T\approx1.6$ in the larger system $L=96$, as discussed in Sec. II D.
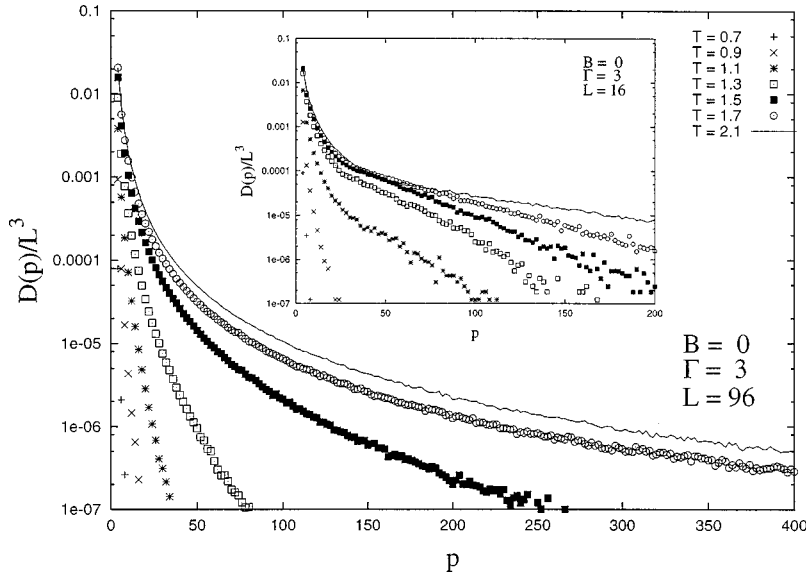
FIG. 5. The distribution function $D(p)/L^3$ of thermally excited closed vortex loops per site as a function of perimeter p, for $B=0$, $\Gamma =3$, $L=96$, and various temperatures. For $T<T_c\simeq 1.6$, $D(p)$ is best fit to an exponential decay. For $T=T_c$, $D(p)$ is best fit to an algebraic decay, $D(p)\sim p^{-\alpha}$, with $\alpha =3$ consistent with critical scaling of Sec. II F. The inset shows the same figure for $L=16$. Note that for $L=16$, $D(p)$ incorrectly shows algebraic decay for $T=1.3<T_c$. This finite-size effect is discussed in Sec. II D.

C. Specific heat

We now present our results for the specific heat in zero magnetic field for the system sizes $L=8,32,64,96$, and consider first the isotropic case $\Gamma =1$.

The specific heat in the isotropic case is shown in Fig. 2. The anomaly in the specific heat clearly correlates with the temperature where the superfluid stiffness vanishes, which in turn correlates precisely with the temperature where the vortex-loop blowout is observed. As the system size increases the anomaly clearly also becomes sharper. We have shown that the peak in the specific heat varies in very good agreement with $\ln(L)$ as the system size is increased, further indicating a genuine thermodynamic phase transition. The shape of the specific-heat curve has a typical XY behavior for this extreme type-II superconductor ($\lambda \rightarrow \infty$). This agrees with previous results found by Dasgupta and Halperin for the lattice superconductor model.[12] (Note that this contrasts sharply with the specific-heat results indicating an *inverted XY* transition found by the same authors for finite, small λ in the isotropic case.) Qualitatively, our results also agree well with the specific-heat measurements on YBCO of Schilling *et al.*[29]

The specific heat for the anisotropic case $\Gamma =3$ is shown in Fig. 3 for the system sizes $L=8$, 32, 64, 96. The situation again at first glance appears to be more complicated than the isotropic case. However, as in the isotropic case, the peak in the specific-heat anomaly increases with system size. Moreover, the temperature of the peak in the specific heat is reduced as the system size is increased, approaching the temperature $T=1.57$ at which both Υ_z and Υ_x vanish, and where the vortex-loop blowout appears to take place.

Hence, our simulations of the above three quantities Υ_z, $D(p)$, and specific heat correctly capture the physics that even in the very anisotropic case, only one single phase transition occurs in the lattice superconductor model in zero magnetic field. The fact that our simulations do not reveal an artificial zero-field decoupling transition due to finite-size ef-

fects, makes us confident that our simulations are able to capture the subtle zero-field physics correctly in the anisotropic case. This is a necessary prerequisite for being able to extract meaningful results from our finite-field simulations, to which we now turn.

IV. RESULTS, FINITE MAGNETIC FIELD

Next, we present results for finite magnetic induction. We will consider the filling fraction $f=\frac{1}{32}$ corresponding to 32 *ab* plane plaquettes per field-induced flux line in the ground state, depicted in Fig. 1. Again, we are primarily interested in correlating temperatures where the helicity moduli vanish with temperatures where anomalies in specific heat occur, as well as with temperatures where we see a qualitative change in the distribution of non-field-induced closed vortex loops. It is also of interest to correlate these phenomena with the melting of the FLL as evidenced by a drop in the structure function at low-order Bragg peaks. Furthermore, due to the presence of field-induced flux lines, it is also of interest to monitor the amount of flux-line cutting occurring in the system. This has bearing on the amount of entanglement of flux lines the molten vortex phase can sustain. For finite fields we present results for helicity moduli, vortex-loop distribution, specific heat, structure function and flux-line cutting for the two values of the anisotropy parameter, $\Gamma =1$ and $\Gamma =3$.

A. Structure function

The results for the structure function $S(\mathbf{Q})$ are shown in the top panel of Fig. 6 for the isotropic case $\Gamma =1$, for the reciprocal lattice vector $\mathbf{Q}=(\mathbf{K}_2,k_z=0)$, $\mathbf{K}_2=2\pi[0,\frac{1}{4}]$, and for the system sizes $L=48$, 64, 80, 96. In the top panel of Fig. 7, results for $\Gamma =3$ and for various system sizes $L=32,48$ are also shown. The structure function exhibits a sharp drop at $T=T_m$, well below the temperature where the phase coherence in the direction of the magnetic field van-
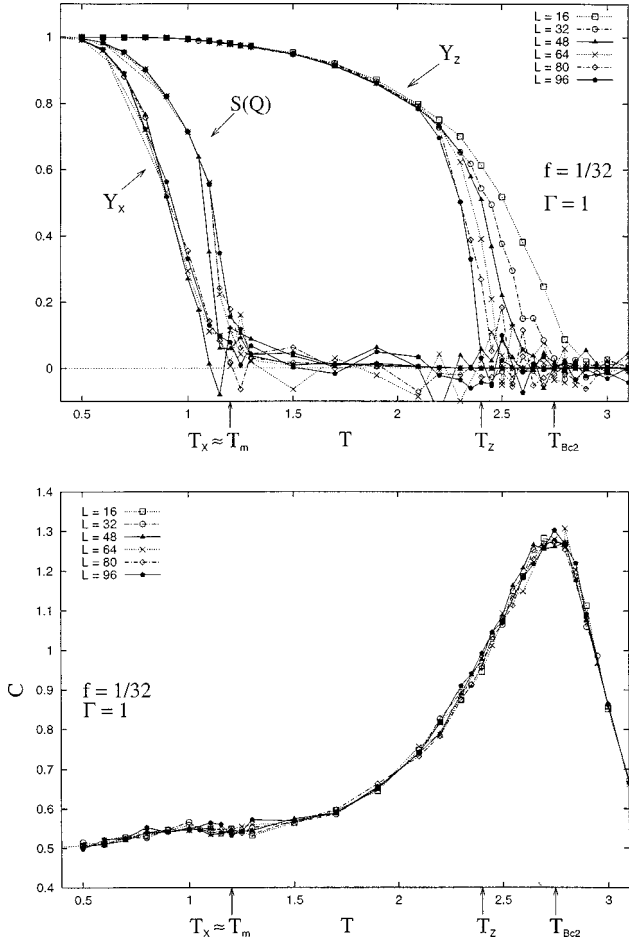
FIG. 6. Top panel: Helicity moduli Y_x and Y_z and structure factor $S(\mathbf{Q})$ vs temperature, for $f=1/32$, $\Gamma=1$, and $L=16,32,48,64,96$. Note how for increasing system size, T_m increases slightly, and T_z decreases markedly. Lower panel: The specific heat per site C vs temperature for $f=1/32$, $\Gamma=1$, and $L=16,32,48,64,96$.

FIG. 7. Top panel: Helicity moduli Y_x and Y_z and structure factor $S(\mathbf{Q})$ vs temperature, for $f=1/32$, $\Gamma=3$, and $L=16,32,48$. Note how for increasing system size, T_m increases slightly and T_z decreases markedly. Lower panel: The specific heat per site C vs temperature for $f=1/32$, $\Gamma=3$, and $L=16,32,48$. Note the two separate specific heat per site anomalies at $T_x=T_m$ and T_z. The specific-heat peak at T_m becomes more prominent with increasing system size, while the peak at T_z actually decreases with increasing system size.

ishes. (We discuss the helicity modulus Y_z in the next section.) Note that the structure function vanishes essentially at the same temperature as the temperature where the helicity modulus Y_x vanishes. What this indicates is that the filling fraction we have used in our simulations, $f=\frac{1}{32}$, is not sufficiently small to study the melting of the FLL in the continuum limit. The FLL has not thermally ''depinned'' from the numerical mesh at the melting transition. Therefore, our estimate for the FLL melting temperature as obtained in these simulations is too high. However, from our earlier work on the moderately anisotropic lattice London model,[11] we know that $f=\frac{1}{48}$ suffices to produce a thermal ''depinning'' temperature of the FLL off the numerical mesh at a temperature distinctly below the observed melting temperature of the FLL. Therefore, we expect that the present estimate for T_m should be quite good; only a minor reduction of the filling fraction below $f=\frac{1}{32}$ is expected to suppress the ''depinning'' temperature T_x below the melting temperature T_m. It is also possible that the commensuration effect might tend to overestimate a first-order character of the FLL melting transition, should such a result be found.

The reduction in the structure function below the melting temperature is due to the Debye-Waller (DW) factor

$$S(\mathbf{Q},T)=S(\mathbf{Q},0)\exp(-G^2\langle u^2\rangle). \tag{8}$$

For a triangular lattice, we find right below the melting transition

$$S(\mathbf{Q},T)=S(\mathbf{Q},0)\exp\left(-\frac{8\pi}{3}c_L^2\right), \tag{9}$$

where c_L is the Lindemann ratio. In our simulation, we find that the DW factor is 0.6 right below the melting transition, and hence $c_L=0.24$. Essentially the same result is found for the isotropic case, and is in reasonable agreement with the value $c_L=0.4$ used in the best calculation so far to estimate the position of the FLL melting line in BSCCO and YBCO by employing the simple Lindemann criterion in conjunction with the highly nontrivial fluctuation propagator found from anisotropic and nonlocal elastic theory of the flux-line lattice.[31]
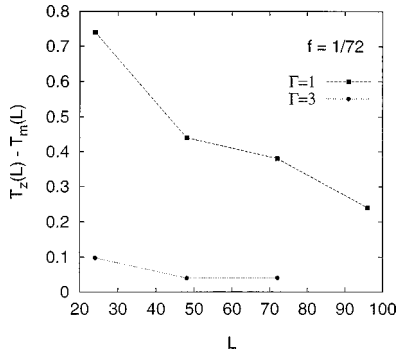
FIG. 8. The difference $T_z(L) - T_m(L)$ as a function of L for $f = 1/72$, $\Gamma = 1$, and $\Gamma = 3$. Note that this quantity shows a monotonically (sublinear) decrease with L. Note also that the relative decrease is larger for $\Gamma = 1$ than for $\Gamma = 3$. We attribute this to a slower relaxation in the anisotropic case than in the isotropic, since both T_m and T_z are smaller for $\Gamma = 3$ than for $\Gamma = 1$.

B. Helicity modulus

The results for the helicity moduli Y_z and Y_x are shown for $\Gamma = 1$ and system sizes $L = 16, 32, 48, 64, 80, 96$ in the top panel of Fig. 6. Likewise, similar results for $\Gamma = 3$ are shown in the top panel of Fig. 7 for system sizes $L = 16, 32, 48$. Note how the temperature T_z appears to decrease monotonically with system size.

An important issue is how T_z will continue to vary when the system size is increased indefinitely. Since there is no obvious sign of saturation in T_z as L increases, it could conceivably continue to decrease in the liquid phase, until it reaches T_m. Does this in fact happen, or is $T_z > T_M$ in the thermodynamic and continuum limit?

To answer this question, we have performed simulations on systems with filling fractions $f = \frac{1}{72}$, and computed T_m and T_z as a function of L. The point about going to lower filling fractions is that we are approximating the continuum limit better. It is becoming increasingly clear from numerical simulations that when the xy plane is discretized in order to do the simulations one is introducing a long time scale into the problem: There is a gap for moving vorticities from one unit cell to another. When the filling fraction is lowered, the continuum approximation is better approximated, and the relaxation time introduced by discretization is lowered. Hence, for $f = \frac{1}{72}$ we are better able to equilibrate the system. (Incidentally, we believe the reason that no finite-size effect was seen in Y_z in Ref. 17 was precisely that the simulations were not run for a long enough time.) The results of our simulations for this case is shown in Fig. 8, where we show $T_z(L) - T_m(L)$ for $\Gamma = 1$ and $\Gamma = 3$, for the case $f = \frac{1}{72}$. It is seen that $T_z(L) - T_m(L)$ decreases monotonically as a function of L. Is it possible that T_z could drop arbitrarily far below T_m when the anisotropy Γ is increased indefinitely? We believe that the answer for $\lambda = \infty$ is no, for the following reason.

Recall our discussion in Sec. II D, where it was shown that in zero field, no vortex-loop blowout can take place below the zero-field transition temperature, due to the renormalization of the interplane coupling. In finite fields, this is quite different, since the superconducting coherence length is limited by the *magnetic length* as soon as the flux lines start to fluctuate appreciably, cutting off the renormalization of

the interplane phase coupling. Hence, we see that T_z drops well below T_{Bc2}, in finite fields, provided the system is in the liquid phase. In the flux-line *lattice* phase, the coherence length is no longer limited by the magnetic length, there is now phase coherence throughout the sample (but of a more complicated form then in the zero-field case). Hence, the renormalization of the interplane coupling described in Sec. II D again becomes active, suppressing the vortex-loop blowout. The flux-line lattice phase is therefore in some sense equivalent to the zero-field case with regards to a vortex-loop blowout, and a loss of phase coherence along the field direction cannot take place within the lattice phase. *Hence, T_z cannot drop far below T_m*, at least not for the case $\lambda = \infty$.

In our previous work[11] we emphasized the importance of closed loops, but suggested that the drop in Y_z within the liquid phase was a genuine phase transition from a coherent vortex liquid characterized by $Y_z \neq 0$, to an incoherent vortex liquid characterized by $Y_z = 0$. We strongly believe our present simulations on much larger systems show that this in fact is not the case: $T_z \rightarrow T_m$ as the system size increases. However, the final word on the issue, particularly for the isotropic case $\Gamma = 1$, remains to be said.

Note also that, compared to the zero-field case $f = 0$, Y_z vanishes at a considerably lower temperature when $f = \frac{1}{32}$. The helicity modulus Y_x vanishes at a finite temperature below Y_z.

The fact that Y_x vanishes at a finite temperature is an artifact of our discretizing the *ab* plane. In the continuum limit, this helicity modulus would be zero for any finite temperature when no physical pinning of the flux lines is present. On the other hand, Y_z has little or no commensuration effects in it.

The above result indicates that phase coherence across the sample along the direction of the flux lines is lost at a finite temperature T_z. Contrary to the zero-field case, there are several possible explanations for this loss of phase coherence when a finite field is present. One possibility is that a vortex-loop blowout causes the loss of phase coherence at $T = T_z$. Another explanation could be that since the melting temperature T_m is smaller than T_z, in FLL liquid phase flux lines become entangled thereby destroying the phase coherence in the superconducting order parameter along the direction of the flux lines. A third explanation could be that transverse flux-line meanderings and flux-line cutting causes loss of phase coherence without a resulting entanglement of flux lines. We discuss these possibilities in turn.

C. Loop distribution

The results for the distribution of closed vortex loops are shown in Fig. 9, in the temperature range $T \in [0.9, 2.5]$, for the anisotropy $\Gamma = 3$ and the system size $L = 48$. This temperature range encompasses the melting of the FLL and the destruction of phase coherence along the direction of the magnetic field. A feature which distinguishes the finite-field results for $D(p)$ from the zero-field case, is that throughout the temperature range where the FLL melts, $T_m \approx 0.38$ and where phase coherence is lost, $T_z \approx 0.65$, the distribution function $D(p)$ decays more rapidly than at the critical point
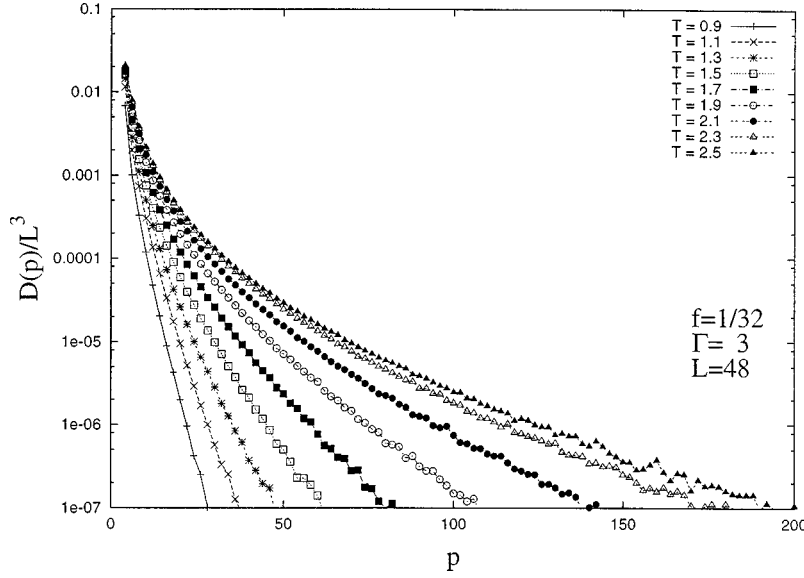
FIG. 9. The distribution function $D(p)/L^3$ of thermally excited closed vortex loops as a function of perimeter p, for $f = 1/32$, $\Gamma = 3$, $L = 48$, and various temperatures. For $T < T_{Bc2} \simeq 1.8$, $D(p)$ is best fit to an exponential decay. For $T > T_{Bc2}$, $D(p)$ is best fit to an algebraic decay, indicating a vortex loop blowout at $T_{Bc2} \gg T_z > T_m$.

in zero field. In the range $T < 0.7$ there is no obvious sign in $D(p)$ of a crossover to algebraic decay as a function of loop perimeters.

We conclude that the vanishing of Υ_z is not, in this case, associated with a vortex-loop blowout on all length scales of the system. In other word, the vanishing of Υ_z is not due to a finite-field counterpart of the Onsager-loop blowout we found in zero field. We find a change in the behavior in $D(p)$ from exponential decay to algebraic decay at a much larger temperature $T \approx 2.8$ for $\Gamma = 1$ and $T \approx 1.9$ for $\Gamma = 3$. The temperature range over which $D(p)$ changes behavior is also considerably broader than in the zero-field case, indicating that the vortex-loop blowout transition that was found to be sharp at zero field, is replaced by a crossover.

However, the interaction between closed vortex loops and the flux-line lattice may be studied by considering the number of closed vortex loops with a diameter given by the magnetic length in the problem. This number scales with L_z at T_z, and thus in the thermodynamic limit there are infinitely many such vortex loops per flux line at the temperature where the FLL melts.

D. Specific heat

Our results for the specific heat are shown in the bottom panel of Fig. 6 for the parameters $f = \frac{1}{32}$, $\Gamma = 1$ and $L = 16,32,48,64,80,96$. Similar results for the anisotropic case $\Gamma = 3$ are shown in the bottom panel of Fig. 7. It is clear that the lowest anomaly in the specific heat correlates with the melting of the FLL. There is also a broad feature at a much higher temperature, $T_{Bc2} \approx 1.9$, which is roughly equal to the temperature at which we see a sharp peak in the specific heat in the zero-field case.

The feature at T_{Bc2} is the remnant of the zero-field anomaly on the specific heat, previously shown in Fig. 3. This broad peak in the specific heat is associated with the upper critical field $H_{c2}(T)$, and our results show that in the extreme type-II Villain model, the $H_{c2}(T)$ line is very steep

close to the zero-field T_c. As discussed in the previous section, T_{Bc2} is also close to the temperature at where the distribution function $D(p)$ of closed vortex loops changes behavior for exponential to algebraic decay. Hence, we conclude that in the field regime corresponding to $f = \frac{1}{32}$, the loop transition appears close to the mean-field $H_{c2}(T)$ line. We caution the reader that $f = \frac{1}{32}$ is not a particularly low magnetic field. If we estimate it for YBCO using the method of Ref. 9, it corresponds to a magnetic field of the order of 1 T. As recently emphasized by Tešanović[10] and Nguyen, Sudbø, and Hetzel[11] such magnetic fields may not be relevant for discussing the low-field experiments of Zeldov et al.[4] Therefore, our simulations do not address the issue of the fate of the zero-field loop transition in asymptotically low magnetic fields, of the order of 100 G and below. Neither do the simulations address how this finite-field counterpart of the zero-field vortex-loop transition interacts with the melting transition of the FLL and with the loss of phase coherence along the field direction, in this low-field regime relevant for discussing the results in Ref. 4.

We next turn to a discussion of the anomalies at the two lower temperatures T_m and T_z, and base our discussion on the lower panel of Fig. 7. It shows the specific heat for the filling $f = \frac{1}{32}$ and anisotropy $\Gamma = 3$, for various system sizes $L = 16,32,48$. The feature in the specific heat at $T = T_m$ is clearly associated with FLL melting. One notable feature in the specific heat anomaly at $T = T_m$ is that its peak scales as L^3, characteristic of a *first-order* melting transition.[12] This follows from the fact that a first-order phase transition is generally characterized by coexistence of two phases at the transition: one low-energy ordered phase and one high-energy disordered phase. Thus there is a discontinuity in the internal energy of the system at the transition temperature, *and a δ-function peak* in the specific heat. On a finite system the δ-function peak is converted to a peak of order L^d, where L is the linear dimension of the system, and d is its dimensionality. In fact, the coefficient of the L^d term is the discontinuity in the entropy of the system, at the transition,[12] so for the 3D case we obtain
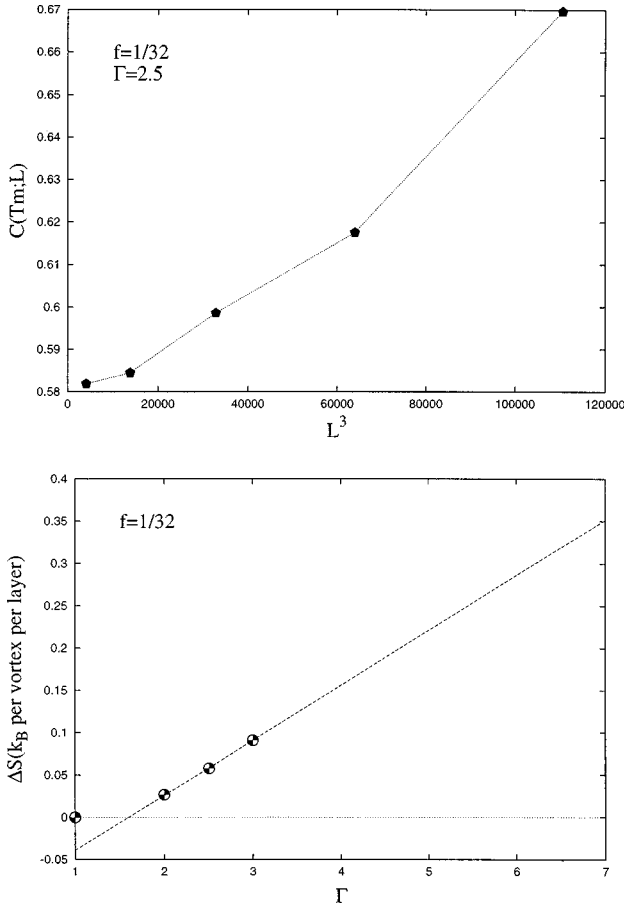
FIG. 10. Top panel: The specific-heat maximum at the flux-line lattice melting transition, as a function of system size, for a given mass anisotropy $\Gamma = 2.5$. Such plots may be used to extract the entropy discontinuity at the melting transition, as explained in the text. Bottom panel: Entropy discontinuity at the melting transition as a function of mass anisotropy. The first order character of the flux-line lattice melting is seen to increase rapidly with increasing Γ.

$$C = \text{const} + \frac{L^3}{4} \left(\frac{\Delta S}{k_B L^3} \right)^2 .$$

Thus we may use finite-size scaling of the specific heat to extract ΔS, or equivalently, the latent heat of the melting transition. We find

$$\Delta S \approx 0.00 k_B / \text{vortex per layer}, \quad \Gamma = 1.0,$$

$$\Delta S \approx 0.03 k_B / \text{vortex per layer}, \quad \Gamma = 2.0,$$

$$\Delta S \approx 0.05 k_B / \text{vortex per layer}, \quad \Gamma = 2.5,$$

$$\Delta S \approx 0.10 k_B / \text{vortex per layer}, \quad \Gamma = 3.0.$$

The results for a finite-size scaling of the specific heat per site C and the entropy discontinuity at the melting transition, are shown in Fig. 10. Δ is seen to increase rapidly with Γ. This is expected on general grounds, since the flux-line liquid in a very anisotropic superconductor is expected to exhibit more disorder than in an isotropic case due to the more flexible nature of *individual* flux lines in layered compounds. In our opinion, a reduction of ΔS with increasing Γ would be

unphysical, at least in situations where the superconductor can be viewed as an anisotropic continuum. The 2D case is in some sense a singular limit, as discussed in Sec. II D. Although it is expected on general grounds that the melting of the FLL is first order also in the isotropic case, it appears to be too small to detect in our simulations. However, by extrapolation we may easily extract entropy jumps of the correct order of magnitude seen in calorimetric data on YBCO with $\Gamma \approx 8$,[7] since ΔS is expected to grow with further increase in Γ. If we extrapolate our results to $\Gamma = 7$, we obtain the value $\Delta S = 0.35 k_B$/per vortex per layer, in very good agreement with experimental data on YBCO. This estimate is again in surprisingly good agreement with, and only slightly larger than, the result obtained by Hetzel and co-workers for the uniformly frustrated 3D XY model[9] with a considerably more sophisticated technique, but where the effect of anisotropy was not fully accounted for.

There is also a weak specific-heat anomaly at $T = T_z$, associated with the loss of phase coherence in the BCS order parameter along the field direction. What this specific-heat anomaly conceivably could show, is that there is a phase transition inside the flux-line liquid phase, from a low-temperature flux-line liquid phase, to a high-temperature flux-line liquid phase, as suggested by Feigel'man *et al.*[32] In Ref. 32, the low-temperature phase is suggested to correspond to a flux-line liquid with no entanglement of flux lines, while the high-temperature flux-line liquid phase is suggested to correspond to a flux-line liquid with entanglement. In the language of the 2D boson analogy,[33] the former would correspond to a normal Bose liquid, while the latter would correspond to a superfluid Bose liquid, the two being separated by a genuine phase transition.

Note however, that the temperature T_z goes down with increasing system size, apparently with no sign of saturation, approaching T_m from above. What this strongly indicates, is that the portion of the phase diagram with a flux-line liquid phase with an apparent intact phase coherence in the BCS order parameter across the sample parallel to the magnetic field, will vanish in the thermodynamic limit.

The question remains as to what the character of the flux-line liquid phase with no phase coherence along the magnetic field, is. We have addressed the issue of whether the transition at $T_z \rightarrow T_m$ results in a flux-line liquid with well-defined flux lines, by considering the amount of flux-line cutting and intersectioning of flux lines with closed vortex loops, that takes place below and above the temperature $T_z \rightarrow T_m$.

E. Flux-line cutting

A flux-line liquid with large amounts of flux-line cutting events, is not likely to be able to sustain a heavily entangled vortex configuration with well-defined flux lines. The amount of flux-line intersectioning, ρ, Eq. (7), is shown in Fig. 11. As we see, ρ increases sharply from zero at $T = T_z$, and continues to increase monotonically as a function of temperature. Flux-line cutting is an efficient way of disentangling flux lines, and the large values of ρ suggest that in the flux-line liquid phase, above T_z, the flux-line liquid is incapable of sustaining an entangled configuration. Hence, the loss of phase coherence along the direction of the magnetic field essentially is due to intersectioning between flux
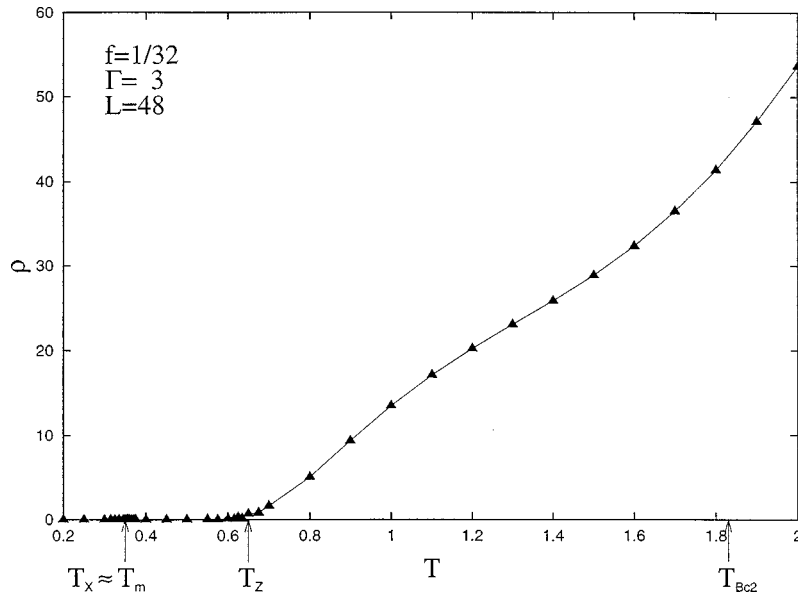
FIG. 11. The number of vortex-intersection events per flux line ρ, for $f = 1/32$, $\Gamma = 3$, and $L = 48$.

lines, and between flux lines and vortex loops, with associated massive flux-line recombinations. Recall that $T = T_z$ is also the temperature at which the number of closed vortex loops of diameter equal to the magnetic length in the problem starts scaling with L_z, and it is natural to associate the increase in ρ with this limited proliferation of vortex loops in a finite field. Under such circumstances, a world-line picture of 2D bosons appears unlikely to be a particularly useful analogy to the flux-line liquid system.

V. SUMMARY

As discussed in Sec. II C, there can only be one single 3D phase transition in the superconductor in zero field, regardless of the anisotropy as long as this is finite, $\Gamma < \infty$. We have shown that in zero field, the superconductor–normal-metal transition is due to a vortex-loop transition analogous to that first suggested to occur in neutral superfluids, such as He[4], by Onsager.[13] The transition is characterized by a vanishing vortex-loop line tension, giving a loop-distribution function that decays as $r^{-\alpha}$ at the transition, where r is the radius of the loop. Below T_c, the decay of the loop-distribution function clearly appears to be faster-than-algebraic. If the anisotropy is increased the vortex-loop unbinding temperature is reduced, but the transition remains 3D. Close to the transition the system is isotropized due to an upward renormalization of the interplane coupling as a consequence of a diverging superconducting coherence length at the transition.

An important point is that in finite magnetic fields, the situation is qualitatively different. In this case, the magnetic length of the vortex system, i.e., the average distance between the flux lines, cuts off the upward renormalization of the interplane coupling.[10,11] Note that the magnetic length only sets a new length scale for the phase coherence *as long as the flux lines actually fluctuate*. In the ground state, with no fluctuations in the Abrikosov vortex lattice, the zero-field arguments apply.[11]

Therefore, the perfect Abrikosov vortex lattice has no effect on the vortex-loop blowout transition, since the phase coherence length is essentially infinite for this case. Consequently, for the case $\lambda = \infty$, one cannot have a vortex-loop blowout transition far below the flux-line lattice melting temperature.

As soon as the flux lines start to fluctuate appreciably, which only happens very close to the melting transition due to the first-order character of the transition, the resulting much smaller cutoff on the renormalization of the interplane coupling facilitates a vortex-loop blowout virtually at the same temperature as the flux lines start to fluctuate. We emphasize that these statements apply to the case of total suppression of gauge fluctuations, or $\lambda = \infty$. Even if vortex loops do not exist on all length scales in the problem at the flux-line lattice melting temperature, they will seriously affect the flux-line liquid phase provided that they exist on length scales up to the magnetic length of the problem. *From our simulations, we have found that this is always the case in the thermodynamic limit*: The number of such non-field-induced closed vortex-loops scales with the thickness of the sample, L_z, whereas the number of field-induced flux lines obviously does not. Therefore there is an infinite number of closed vortex loops with a diameter equal to the magnetic length, per flux line. Hence, in the liquid phase flux lines cannot be considered as well-defined entities. They are well-defined entities in the *lattice case*.

When a flux-line lattice melts, the molten phase is an *incoherent vortex-liquid* characterized by loss of phase coherence along the direction of the magnetic field. This loss of phase coherence is associated with a proliferation of closed vortex loops and massive flux-line cutting and recombination. Such a vortex-liquid phase is unlikely to sustain heavily entangled vortex configurations. Recent works from Hu, Miyashita, and Tachiki,[34] as well as from Koshelev,[35] support the conclusion that $T_z = T_m$ when $\lambda = \infty$, at least in the field regime considered, i.e., $f = \frac{1}{25}$ (Ref. 34) and $f = \frac{1}{36}$.[35]

APPENDIX A: HELICITY MODULUS IN TERMS OF PHASE VARIABLES

In this appendix we derive the expression for the helicity modulus Y_μ (Eq. 6), for the uniformly frustrated *anisotropic* Villain model. The effective Hamiltonian for the uniformly frustrated anisotropic Villain model is

$$H_v\{\theta'(\mathbf{r})\} = J_0 \sum_{\mathbf{r}, \nu=x,y,z} V_\nu[\theta'(\mathbf{r}+\hat{e}_\nu) - \theta'(\mathbf{r}) - A_\nu(\mathbf{r})],$$

$$V_\nu(\chi) = -\frac{k_B T}{J_0} \ln\left\{ \sum_{m=-\infty}^{\infty} \exp\left[-\frac{J_0 \alpha_\nu}{2k_B T} (\chi - 2\pi m)^2 \right] \right\}. \tag{A1}$$

Here, J_0, $A_\nu(\mathbf{r})$, and α_ν are defined in the text, $\hat{e}_\nu$ is the unit vector for the $\hat{\nu}$ axis. In Eq. (A1), $\theta'(\mathbf{r})$ is the phase of the complex superconducting order parameter. $\{\theta'(\mathbf{r})\}$ denotes the functional of $\theta'(\mathbf{r})$. We now apply boundary conditions such that the phase across the system in the $\hat{\mu}$ direction is twisted by an amount $L\delta$. If $\hat{\mu} = \hat{z}$, for example, we have the following phase twist:

$$\theta'(x,y,z=L) - \theta'(x,y,z=0) = L\delta. \tag{A2}$$

Now we define a set of new phase variables

$$\theta(\mathbf{r}) = \theta'(\mathbf{r}) - (\mathbf{r} \cdot \hat{e}_\mu)\delta.$$

If the phase variables $\theta'(\mathbf{r})$ obey the twisted boundary conditions in Eq. (A2), the new phase variables $\theta(\mathbf{r})$ obey the following periodic boundary conditions:

$$\theta(x,y,z=L) - \theta(x,y,z=0) = 0. \tag{A3}$$

The Hamiltonian for the uniformly frustrated anisotropic Villain model in terms of the new phase variables is

$$H_v\{\theta,\delta\} = J_0 \sum_{\mathbf{r}, \nu=x,y,z} V_\nu[\theta(\mathbf{r}+\hat{e}_\nu) - \theta(\mathbf{r}) - A_\nu(\mathbf{r})$$
$$+ (\hat{e}_\nu \cdot \hat{e}_\mu)\delta].$$

The partition function in terms of the new phase variables is

$$Z(\delta) = \sum_{\{\theta(\mathbf{r})\}} e^{-H_v\{\theta(\mathbf{r}),\delta\}/k_B T},$$

where we only sum over configurations $\{\theta(\mathbf{r})\}$ that satisfy periodic boundary conditions. The total free energy is

$$F(\delta) = -k_B T \ln Z(\delta).$$

The helicity modulus Y_μ is defined as the second derivative of the free energy with respect to a phase twist across the sample in the $\hat{\mu}$ direction. Thus,

$$Y_\mu \equiv \frac{1}{L^3} \left(\frac{\partial^2 F(\delta)}{\partial \delta^2} \right)_{\delta=0}.$$

Using the definition

$$\chi \equiv \theta(\mathbf{r}+\hat{e}_\nu) - \theta(\mathbf{r}) - A_\nu(\mathbf{r}) + (\hat{e}_\nu \cdot \hat{e}_\mu)\delta,$$

$$\frac{\partial \chi}{\partial \delta} = \hat{e}_\nu \cdot \hat{e}_\mu.$$

we can write Y_μ in the following form:

$$Y_\mu = \frac{J_0^2}{L^3} \frac{1}{k_B T} \left(\frac{\sum_{\{\theta(\mathbf{r})\}} \left[\sum_{\mathbf{r},\nu} \frac{\partial}{\partial \chi} V_\nu(\chi)(\hat{e}_\nu \cdot \hat{e}_\mu) \right] e^{-H_v\{\theta(\mathbf{r})\}/k_B T}}{Z(\delta=0)} \right)^2 + \frac{J_0}{L^3} \frac{\sum_{\{\theta(\mathbf{r})\}} \left[\sum_{\mathbf{r},\nu} \frac{\partial^2}{\partial \chi^2} V_\nu(\chi)(\hat{e}_\nu \cdot \hat{e}_\mu)^2 \right] e^{-H_v\{\theta(\mathbf{r})\}/k_B T}}{Z(\delta=0)}$$

$$- \frac{J_0^2}{L^3} \frac{1}{k_B T} \frac{\sum_{\{\theta(\mathbf{r})\}} \left[\sum_{\mathbf{r},\nu} \frac{\partial}{\partial \chi} V_\nu(\chi)(\hat{e}_\nu \cdot \hat{e}_\mu) \right]^2 e^{-H_v\{\theta(\mathbf{r})\}/k_B T}}{Z(\delta=0)},$$

which is Eq. (6) written in a more explicit form. The summations over the configurations $\{\theta(\mathbf{r}_i)\}$ are restricted to configurations satisfying periodic boundary conditions.

APPENDIX B: HELICITY MODULUS IN TERMS OF VORTEX SEGMENTS CORRELATIONS

In this appendix we derive the helicity modulus for the anisotropic LSM $Y_\mu(\mathbf{k})$, expressed in terms of vortex density-density correlation functions (Ref. 11), $\mu=(x,y,z)$. In the continuum limit, the effective Hamiltonian for the anisotropic LSM can be written as

$$H\{\mathbf{v},\mathbf{f}\} = \frac{J_1}{2} \int d^3r [\mathbf{v}(\mathbf{r}) \cdot \overset{\leftrightarrow}{M} \cdot \mathbf{v}(\mathbf{r}) + 2\pi\lambda^2 \mathbf{f}(\mathbf{r}) \cdot \mathbf{f}(\mathbf{r})], \tag{B1}$$

the energy per unit length $J_1 = \Phi_0^2/16\pi^3\lambda_a^2$. Here, $\mathbf{v}(\mathbf{r})$ is the superfluid velocity

$$\mathbf{v}(\mathbf{r}) = \nabla\theta(\mathbf{r}) - \mathbf{A}(\mathbf{r}),$$

$\theta(\mathbf{r})$ is the phase of the complex superconducting order parameter, $\Phi_0\mathbf{A}(\mathbf{r})/2\pi$ is the vector potential, and Φ_0 is the flux quantum. In Eq. (B1), $\overset{\leftrightarrow}{M}$ is the anisotropic mass tensor,

$$\overleftrightarrow{M} = \begin{bmatrix} 1 & 0 & 0 \\ 0 & 1 & 0 \\ 0 & 0 & \Gamma^2 \end{bmatrix},$$

describing uniaxial $\hat{c}$ anisotropy. The anisotropy parameter $\Gamma = \lambda_c / \lambda_a$, λ_a and λ_c are explained in the text. In Eq. (B1), $\mathbf{f}(\mathbf{r})$ is the local density of the magnetic flux quanta,

$$\mathbf{f}(\mathbf{r}) = \frac{\mathbf{B}(\mathbf{r})}{\Phi_0} = \frac{1}{2\pi} \boldsymbol{\nabla} \times \mathbf{A}(\mathbf{r}).$$

Here, $\mathbf{B}(\mathbf{r})$ is the local magnetic induction. In evaluating Eq. (B1), the integration must be cutoff at the core of the vortex segments, so that the energy stays finite.

The partition function Z is computed averaging over independently fluctuating $\mathbf{v}(\mathbf{r})$ and $\mathbf{f}(\mathbf{r})$, subject to the constraint $\langle \mathbf{f}(\mathbf{r}) \rangle = f\hat{e}_z$ for a constant uniform average magnetic induction $B\hat{e}_z$, where $\langle \dots \rangle$ denotes a thermal average, and $\hat{e}_\mu$ is the unit vector along the $\hat{\mu}$ axis. Using the Fourier transform

$$\widetilde{v}(\mathbf{k}) = \int d^3 r\, e^{i\mathbf{k}\cdot\mathbf{r}} \mathbf{v}(\mathbf{r}),$$

the Hamiltonian in Eq. (B1) can be written as

$$H\{\mathbf{v}(\mathbf{k}), \widetilde{f}(\mathbf{k})\} = \frac{J_1}{2V} \sum_k H'(\mathbf{k}),$$

$$H'(\mathbf{k}) = [\widetilde{v}(\mathbf{k})\cdot\overleftrightarrow{M}\cdot\widetilde{v}(-\mathbf{k}) + 2\pi\lambda^2 \widetilde{f}(\mathbf{k})\cdot\widetilde{f}(-\mathbf{k})],$$
$$\tag{B2}$$

where V is the volume of the system. An applied twist in the phase of the superconducting order parameter, along the $\hat{\mu}$ direction, as considered in the previous Appendix, corresponds to a change in the superfluid velocity

$$\widetilde{v}(\mathbf{k}) \rightarrow \widetilde{v}(\mathbf{k}) + \delta v(\mathbf{k})\hat{e}_\mu.$$

In terms of velocities, therefore, the helicity modulus $\Upsilon_\mu(\mathbf{k})$ is defined as the second derivative of the free energy $F = -k_B T \ln Z$ with respect to a change in the superfluid velocity along the $\hat{\mu}$ direction. Hence,

$$\Upsilon_\mu(\mathbf{k}) \equiv \left. \frac{\partial^2 F}{\partial[\delta v(\mathbf{k})]\partial[\delta v(-\mathbf{k})]} \right|_{\delta v(\mathbf{k}) = \delta v(-\mathbf{k}) = 0}$$

$$= \frac{J_1}{V}\left(\hat{e}_\mu \cdot \overleftrightarrow{M} \cdot \hat{e}_\mu - \frac{J_1}{k_B T V} \langle [\widetilde{v}(\mathbf{k})\cdot\overleftrightarrow{M}\cdot\hat{e}_\mu] \right.$$

$$\left. \times [\hat{e}_\mu \cdot \overleftrightarrow{M} \cdot \widetilde{v}(-\mathbf{k})] \rangle_0 \right). \tag{B3}$$

The subscript 0 denotes the unperturbed system with no applied phase twist, $\delta v(\mathbf{k}) = 0$. In Eq. (B3), we have used $\langle \widetilde{v}(\mathbf{k}) \rangle_0 = \langle \widetilde{v}(-\mathbf{k}) \rangle_0 = 0$, since the Hamiltonian Eq. (B2) contains only quadratic terms like $[v_\nu(\mathbf{k})v_\nu(-\mathbf{k})]$ ($\nu = x, y, z$). Because of the symmetry in which $\boldsymbol{\nabla}\theta$ and $\mathbf{A}$ enter $\mathbf{v}(\mathbf{r})$, $\Upsilon_\mu(\mathbf{k})$ can also be interpreted as the linear response coefficient of the supercurrent induced by a perturbation in the vector potential,[27]

$$j_\mu(\mathbf{k}) = -\Upsilon_\mu(\mathbf{k})\delta A_\mu(\mathbf{k}).$$

There are three interesting helicity moduli to be considered: (1) $\Upsilon_x(k\hat{e}_y)$, which is the energy cost corresponding to a compressional perturbation of the flux-line system, (2) $\Upsilon_x(k\hat{e}_z)$, which is the energy cost corresponding to a tilting perturbation of the flux-line system, and (3) $\Upsilon_z(k\hat{e}_x)$, which is the energy cost corresponding to a shearing of the flux-line system.

To find an expression for $\Upsilon_\mu(k\hat{e}_\nu)$ ($\mu \neq \nu$) expressed in terms of vortex segments density correlations, we need to write the parts of H containing $k\hat{e}_\nu$ in a diagonal form. Defining the vortex segment density

$$\mathbf{n}(\mathbf{r}) = \frac{1}{2\pi}\boldsymbol{\nabla}\times\boldsymbol{\nabla}\theta,$$

we can write the superfluid velocity in the following gauge-invariant form:[27]

$$\widetilde{v}(\mathbf{k}) = 2\pi i\left(\mathbf{k}\chi(\mathbf{k}) + \frac{\mathbf{k}\times[\mathbf{n}(\mathbf{k})-\mathbf{f}(\mathbf{k})]}{k^2} \right). \tag{B4}$$

Here, $\chi(\mathbf{r})$ is a smooth scalar function which describes the longitudinal part of $\widetilde{v}(\mathbf{k})$. The transverse part of $\widetilde{v}(\mathbf{k})$ is determined by $\boldsymbol{\nabla}\times\mathbf{v}(\mathbf{r}) = 2\pi[\mathbf{n}(\mathbf{r})-\mathbf{f}(\mathbf{r})]$.

Substituting Eq. (B4) into $H'(\mathbf{k})$ [Eq. (B2)], we get the following diagonal form for $H'(\mathbf{k})$ for the case of $\mathbf{k} = k\hat{e}_\nu$:

$$\frac{H'(k\hat{e}_x)}{4\pi^2} = k^2\chi(k\hat{e}_x)\chi(-k\hat{e}_x) + A_1(k)n_y(k\hat{e}_x)n_y(-k\hat{e}_x) + A_2(k)n_z(k\hat{e}_x)n_z(-k\hat{e}_x) + B_1(k)\delta f_y(k\hat{e}_x)\delta f_y(-k\hat{e}_x)$$

$$+ B_2(k)\delta f_z(k\hat{e}_x)\delta f_z(-k\hat{e}_x),$$

$$\frac{H'(k\hat{e}_y)}{4\pi^2} = k^2\chi(k\hat{e}_y)\chi(-k\hat{e}_y) + A_1(k)n_x(k\hat{e}_y)n_x(-k\hat{e}_y) + A_2(k)n_z(k\hat{e}_y)n_z(-k\hat{e}_y) + B_1(k)\delta f_x(k\hat{e}_y)\delta f_x(-k\hat{e}_y)$$

$$+ B_2(k)\delta f_z(k\hat{e}_y)\delta f_z(-k\hat{e}_y),$$

$$\frac{H'(k\hat{e}_z)}{4\pi^2} = (k/\Gamma)^2\chi(k\hat{e}_z)\chi(-k\hat{e}_z) + A_2(k)n_x(k\hat{e}_z)n_x(-k\hat{e}_z) + A_2(k)n_y(k\hat{e}_z)n_y(-k\hat{e}_z) + B_2(k)\delta f_x(k\hat{e}_z)\delta f_x(-k\hat{e}_z)$$

$$+ B_2(k)\delta f_y(k\hat{e}_z)\delta f_y(-k\hat{e}_z). \tag{B5}$$

Here,

$$A_1(k) = \frac{\lambda^2}{1+\Gamma^2\lambda^2 q^2}, \quad A_2(k) = \frac{\lambda^2}{1+\lambda^2 q^2},$$

$$B_1(k) = \frac{1+\Gamma^2\lambda^2 q^2}{\Gamma^2 q^2}, \quad B_2(k) = \frac{1+\lambda^2 q^2}{q^2}.$$

In Eq. (B5), $\delta\widetilde{f}(\mathbf{k}) = \widetilde{f}(\mathbf{k}) - \widetilde{f}^0(\mathbf{k})$ is the fluctuation of the magnetic flux density away from the value $\widetilde{f}^0(\mathbf{k})$ minimizing the Hamiltonian for a given vortex segments configuration.[36]

$$\widetilde{f}^0(\mathbf{k}) = \frac{\widetilde{n}(\mathbf{k})}{1+\lambda^2 k^2} - \frac{(\Gamma^2-1)[\widetilde{n}(\mathbf{k})\cdot\mathbf{q}]\lambda^2\mathbf{q}}{1+\lambda^2 k^2+(\Gamma^2-1)\lambda^2 q^2},$$

where $\mathbf{q} = \mathbf{k}\times\hat{z}$. To compute the partition function Z, we should sum over (1) all smooth functions $\chi(\mathbf{r})$, (2) all $\widetilde{n}(\mathbf{k})$ that satisfy $\mathbf{k}\cdot\widetilde{n}(\mathbf{k}) = 0$, and (3) all $\delta\widetilde{f}(\mathbf{k})$ that satisfy $\mathbf{k}\cdot\delta\widetilde{f}(\mathbf{k}) = 0$. The constraints (2) and (3) come from the restriction of no divergence in the vortex segments density and no divergence in the local magnetic-field induction. Substituting Eq. (B4) into Eq. (B3), and using the the Hamiltonian

Eq. (B5) to evaluate the average over $\chi(\mathbf{k})$ and $\delta\widetilde{f}(\mathbf{k})$. For the case of $\mathbf{k} = k\hat{e}_\nu$ we obtain

$$\Upsilon_\mu(k\hat{e}_\nu) = \frac{J_1}{V}\frac{\lambda^2 k^2}{1+[1+\delta_{\mu,z}(\Gamma^2-1)]\lambda^2 k^2}$$
$$\times\left(1 - \frac{4\pi J_1}{k_B T V}\frac{\lambda^2\langle n_\sigma(k\hat{e}_\nu)n_\sigma(-k\hat{e}_\nu)\rangle_0}{1+[1+\delta_{\mu,z}(\Gamma^2-1)]\lambda^2 k^2}\right),$$
(B6)

(μ,ν,σ) are cyclic permutation of (x,y,z). The generalization of Eq. (B6) to a lattice superconductor is

$$\Upsilon_\mu(k\hat{e}_\nu) = \frac{J_0}{L^3}\frac{(\lambda/d)^2 Q^2}{1+[1+\delta_{\mu,z}(\Gamma^2-1)](\lambda/d)^2 Q^2}$$
$$\times\left(1 - \frac{4\pi J_0}{k_B T L^3}\frac{(\lambda/d)^2\langle n_\sigma(k\hat{e}_\nu)n_\sigma(-k\hat{e}_\nu)\rangle_0}{1+[1-\delta_{\mu,z}(\Gamma^2-1)](\lambda/d)^2 Q^2}\right),$$
(B7)

where $Q_\mu = 2\sin(k_\mu d/2)$, $Q^2 = \Sigma_\mu Q_\mu^2$, k_μ is the μ component of $\mathbf{k}$, and d is the lattice constant of the (simple cubic) underlying numerical lattice.

[1] H. Safar, P. L. Gammel, D. A. Huse, D. J. Bishop, J. P. Rice, and D. M. Ginsberg, Phys. Rev. Lett. **69**, 824 (1992).

[2] H. Pastoriza, M. F. Goffman, A. Arribére, and F. de la Cruz, Phys. Rev. Lett. **72**, 2951 (1994).

[3] R. A. Doyle, D. Liney, W. S. Seow, A. M. Campbell, and K. Kadowaki, Phys. Rev. Lett. **75**, 4520 (1995).

[4] E. Zeldov, D. Majer, M. Konczykowski, V. B. Geshkenbein, V. M. Vinokur, and H. Shtrikman, Nature (London) **375**, 373 (1995); N. Morozov, E. Zeldov, D. Majer, and M. Konczykowski, Phys. Rev. B **54**, R3784 (1996).

[5] T. Nishikazi, Y. Onodera, N. Kobayashi, H. Asaoka, and H. Takei, Phys. Rev. B **53**, 82 (1996).

[6] U. Welp, J. A. Fendrich, W. K. Kwok, G. W. Crabtree, and B. W. Veal, Phys. Rev. Lett. **76**, 4809 (1996).

[7] A. Schilling, R. A. Fisher, N. E. Phillips, U. Welp, D. Dasgupta, W. K. Kwok, and G. W. Crabtree, Nature (London) **382**, 791 (1996).

[8] A. Junod, M. Roulin, J.-Y. Genoud, B. Revaz, A. Erb, and E. Walker, Physica C **275**, 245 (1997).

[9] R. E. Hetzel, A. Sudbø, and D. A. Huse, Phys. Rev. Lett. **69**, 518 (1992).

[10] Z. Tešanović, Phys. Rev. B **51**, 16 204 (1995).

[11] A. K. Nguyen, A. Sudbø, and R. E. Hetzel, Phys. Rev. Lett. **77**, 1592 (1996).

[12] C. Dasgupta and B. I. Halperin, Phys. Rev. Lett. **47**, 1556 (1981).

[13] L. Onsager, Nuovo Cimento Suppl. **6**, 249 (1949); R. P. Feynman, in *Progress in Low Temperature Physics*, edited by C. J. Gorter (North-Holland, Amsterdam, 1955), Vol. 1, p. 17.

[14] G. Williams, Phys. Rev. Lett. **59**, 1926 (1987); B. Chattopadhyay and S. R. Shenoy, *ibid.* **72**, 400 (1994); W. Janke and T. Matsui, Phys. Rev. B **42**, 10 673 (1990).

[15] S. E. Korshunov, Europhys. Lett. **11**, 757 (1990).

[16] T. Chen and S. Teitel, Phys. Rev. B **55**, 11 766 (1997).

[17] Ying-Hong Li and S. Teitel, Phys. Rev. B **47**, 359 (1993); *ibid.* **49**, 4136 (1994).

[18] E. Frey, D. R. Nelson, and D. S. Fisher, Phys. Rev. B **49**, 9723 (1994).

[19] G. Carneiro, Phys. Rev. B **45**, 2391 (1992).

[20] A. Sudbø and E. H. Brandt, Phys. Rev. Lett. **67**, 3176 (1991); A. Sudbø, E. H. Brandt, and D. A. Huse, *ibid.* **71**, 1451 (1993).

[21] J. Villain, J. Phys. (Paris) **36**, 581 (1975).

[22] B. Horovitz, Phys. Rev. B **47**, 5947 (1993).

[23] J. Friedel, J. Phys. (France) **49**, 1561 (1988); J. Phys.: Condens. Matter **1**, 7757 (1989).

[24] D. R. Nelson and B. I. Halperin, Phys. Rev. Lett. **41**, 121 (1978); *ibid.* **41**, 519 (1978); Phys. Rev. B **19**, 2457 (1979).

[25] A. P. Young, Phys. Rev. B **19**, 1855 (1979).

[26] M. Franz and S. Teitel, Phys. Rev. Lett. **73**, 480 (1994); S. Hattel and J. M. Wheatley, Phys. Rev. B **50**, 16 590 (1994); *ibid.* **51**, 11 951 (1995).

[27] T. Chen and S. Teitel, Phys. Rev. Lett. **72**, 2085 (1994); *ibid.* **74**, 2792 (1995).

[28] This analysis gives the correct exponent for the vortex-antivortex distribution function in the 2D case, where the equilibrium distribution of vortex-antivortex pairs in the presence of a driving current is given by $D(r)\sim r^{-\widetilde{\alpha}}$. It is known that for the 2D case, $\widetilde{\alpha}(T=K_{KT}) = 1+\alpha = 3$, and thus $\alpha = 2$ at the vortex-antivortex unbinding temperature, J. M. Kosterlitz and D. J. Thouless, J. Phys. C **6**, 1181 (1973). For a detailed discussion of the 2D case, see also G. Blatter *et al.*, Rev. Mod. Phys. **66**, 1125 (1994), Sec. 8.

[29] A. Schilling and O. Jeandupeux, Phys. Rev. B **52**, 9714 (1995).

[30] R. Cavalcanti, G. Carneiro, and A. Gartner, Europhys. Lett. **17**, 449 (1992); Phys. Rev. B **47**, 5263 (1993).

[31] A. Houghton, R. A. Pelcovits, and A. Sudbø, Phys. Rev. B **40**, 6763 (1989).

[32] M. V. Feigel'man, V. B. Geshkenbein, L. B. Ioffe, and A. I. Larkin, Phys. Rev. B **48**, 16 641 (1993).

[33] D. R. Nelson, Phys. Rev. Lett. **60**, 1973 (1988); J. Stat. Phys. **57**, 511 (1989); D. R. Nelson and H. S. Seung, Phys. Rev. B **39**, 9153 (1989).

[34] X. Hu, S. Miyashita, and M. Tachiki (unpublished).

[35] A. E. Koshelev (unpublished).

[36] E. H. Brandt, J. Low Temp. Phys. **26**, 735 (1977); A. Sudbø and E. H. Brandt, Phys. Rev. Lett. **66**, 1781 (1991).